© 2021. Published by The Company of Biologists Ltd | Development (2021) 148, dev199166. doi:10.1242/dev.199166

STEM CELLS AND REGENERATION

RESEARCH ARTICLE

Direct repression of *Nanog* and *Oct4* by OTX2 modulates the contribution of epiblast-derived cells to germline and somatic lineage

Luca Giovanni Di Giovannantonio[1,*], Dario Acampora[1,*], Daniela Omodei[1,2], Vincenzo Nigro[3,4], Pasquale Barba[1], Elisa Barbieri[5,6], Ian Chambers[5,6] and Antonio Simeone[1,‡]

ABSTRACT

In mammals, the pre-gastrula proximal epiblast gives rise to primordial germ cells (PGCs) or somatic precursors in response to BMP4 and WNT signaling. Entry into the germline requires activation of a naïve-like pluripotency gene regulatory network (GRN). Recent work has shown that suppression of OTX2 expression in the epiblast by BMP4 allows cells to develop a PGC fate in a precise temporal window. However, the mechanisms by which OTX2 suppresses PGC fate are unknown. Here, we show that, in mice, OTX2 prevents epiblast cells from activating the pluripotency GRN by direct repression of *Oct4* and *Nanog*. Loss of this control during PGC differentiation *in vitro* causes widespread activation of the pluripotency GRN and a deregulated response to LIF, BMP4 and WNT signaling. These abnormalities, in specific cell culture conditions, result in massive germline entry at the expense of somatic mesoderm differentiation. Increased generation of PGCs also occurs in mutant embryos. We propose that the OTX2-mediated repressive control of *Oct4* and *Nanog* is the basis of the mechanism that determines epiblast contribution to germline and somatic lineage.

KEY WORDS: Primordial germ cells, *Otx2*, Pluripotency Gene Regulatory Network

INTRODUCTION

Primordial germ cells (PGCs) represent the founder cells of the germ cell lineage, which ensures the transmission of genetic and epigenetic information across the generations (Wylie, 1999; Surani, 2001; Saitou and Yamaji, 2012; Johnson et al., 2003; Johnson and Alberio, 2015). In mice, both the germline and the somatic lineage, the latter referring to embryonic and extra-embryonic mesoderm (Saitou et al., 2005), originate from the proximal-posterior epiblast of pre-gastrula embryos (Lawson et al., 1999; Saitou, 2009). The generation of PGCs is controlled by a precise mechanism determining the segregation of the germline from the somatic lineage (Ohinata et al., 2009; Surani et al., 2007; Hayashi et al., 2007). The acquisition of PGC identity is associated with loss of somatic mesoderm fate (Günesdogan and Surani, 2016; Saitou et al., 2002). In mouse, germline and somatic lineage originate in response to BMP and WNT signaling (Lawson et al., 1999; Ohinata et al., 2009; Senft et al., 2019). BMP4-mediated activation of the transcription factor (TF) genes *Blimp1* (also known as *Prdm1*), *Ap2γ* (also known as *Tfap2c*) and *Prdm14* is required for germline entry and suppression of somatic mesoderm identity, which is defined by the expression of *T* (also known as *Brachyury*) and *Hoxb1* (Magnúsdóttir et al., 2013; Ohinata et al., 2005; Kurimoto et al., 2008; Ancelin et al., 2006; Vincent et al., 2005; Weber et al., 2010; Yamaji et al., 2008; Nakaki et al., 2013). Co-expression of *Blimp1*, *Ap2γ* and *Prdm14* defines the identity of germ cells *in vivo* and *in vitro*. Further work indicated that WNT3 is also required for PGC fate (Aramaki et al., 2013). Germline entry and development of PGCs also requires the activation of a naïve-like pluripotency gene regulatory network (GRN) defined by the TFs *Oct4* (also known as *Pou5f1*), *Sox2* and *Nanog* and representing a unique feature of the PGC unipotent state (Saitou and Yamaji, 2012; Hayashi et al., 2007; Hackett and Surani, 2014; Leitch et al., 2013; Smith, 2017; Okamura et al., 2008; Yamaguchi et al., 2009; Chambers et al., 2007; Zhang and Chambers, 2019; Campolo et al., 2013; Kehler et al., 2004; Yeom et al., 1996). Importantly, *Nanog* activation in epiblast-like cells (EpiLCs), a cellular state very similar to pre-gastrulation epiblast (Hayashi et al., 2011; Smith, 2017), is sufficient for germ cell induction (Murakami et al., 2016), and *Oct4* expression in PGCs requires a transcriptional regulatory switch from the proximal enhancer (PE) to the distal enhancer (DE) (Choi et al., 2016; Wu and Schöler, 2014). The study of germline development has been fuelled by the realization of a stepwise *in vitro* culture system generating PGC-like cells (PGCLCs) from germline-competent EpiLCs induced, in turn, from naïve embryonic stem cells (ESC) (Hayashi et al., 2011). PGCLCs and PGCs share molecular identity, epigenetic reprogramming and spermatogenic capacity (Hayashi et al., 2011, 2012, 2017). The TF OTX2, a key determinant of brain development (Acampora et al., 1995), is also expressed in pluripotent cells *in vivo* and *in vitro* (Acampora et al., 2013). OTX2 is required to: antagonize naïve pluripotency; promote transition of ESCs from naïve to formative pluripotency; specify the heterogeneous identity of ESCs through reciprocal antagonism with NANOG; and define *in vitro* and *in vivo* naïve-primed intermediate states of pluripotency (Acampora et al., 2013, 2016, 2017; Buecker et al., 2014; Yang et al., 2014; Neagu et al., 2020). Moreover, in pluripotent cells OTX2 may also bind to the enhancer region of *Oct4*, *Nanog* and *Sox2* (Acampora et al., 2016). Recent work has

[1]Institute of Genetics and Biophysics 'Adriano Buzzati-Traverso', CNR, Via P. Castellino, 111, 80131 Naples, Italy. [2]Institute of Biostructures and Bioimaging, CNR, Via Tommaso De Amicis, 95, 80145 Naples, Italy. [3]Dipartimento di Medicina di Precisione, Università degli Studi della Campania 'Luigi Vanvitelli', Via L. De Crecchio, 7, 80138 Naples, Italy. [4]Telethon Institute of Genetics and Medicine (TIGEM), Via Campi Flegrei, 34, 80087 Pozzuoli (NA), Italy. [5]Centre for Regenerative Medicine, Institute for Regeneration and Repair, University of Edinburgh, 5 Little France Drive, Edinburgh EH16 4UU, UK. [6]Institute for Stem Cell Research, School of Biological Sciences, University of Edinburgh, UK.
*These authors contributed equally to this work

‡Author for correspondence (antonio.simeone@igb.cnr.it)

V.N., 0000-0002-3378-5006; A.S., 0000-0003-2693-9836

Handling Editor: Maria Elena Torres-Padilla
Received 7 December 2020; Accepted 12 April 2021

Development (2021) 148, dev199166. doi:10.1242/dev.199166

revealed that OTX2 is a novel crucial determinant controlling germline entry of formative epiblast cells in mouse (Zhang et al., 2018; Zhang and Chambers, 2019; Laird, 2018). Indeed, by restricting germline entry to a limited number of epiblast-derived cells, OTX2 controls segregation of germ cells from somatic precursors. Here, we hypothesized that, mechanistically, entry into germline requires the release by OTX2 of a repressive state preventing activation of the pluripotency GRN in epiblast-derived cells. Our data indicate that, in EpiLC-derived cells, loss of OTX2 binding to *Oct4* or *Nanog* enhancer region causes widespread activation of the pluripotency GRN, increased germline entry and suppression of somatic fate. Generation of PGCs is increased also in mutant embryos. This study uncovers a novel mechanism by which OTX2 regulates epiblast contribution to germline and somatic mesoderm.

RESULTS

OTX2, OCT4 and NANOG expression during PGC development and PGCLC differentiation

To obtain a detailed view of the temporal appearance of OTX2, OCT4 and NANOG relative to germline and somatic differentiation determinants, embryos were analysed by immunofluorescence (Fig. 1A). At embryonic day (E) 6.5, AP2γ and BLIMP1 were co-expressed in a subset of fragilis$^+$ (also known as IFITM3) cells, which included incipient PGCs (Zhang et al., 2018). From E7 to E7.5 these three markers gradually became colocalized in PGCs (yellow arrows in Fig. 1A). At E6.5 and E7, OTX2 was expressed in some fragilis$^+$-AP2γ$^-$ cells (white arrow in Fig. 1A), but became undetectable at E7.5 in fragilis$^+$ cells. During this time window, OCT4 and NANOG were co-expressed in fragilis$^+$ cells, although at E6.5 NANOG was detected at variable levels (Fig. 1A). T was initially expressed throughout the fragilis$^+$ field but by E7.5 disappeared from some fragilis$^+$ cells (Fig. 1A). These data show that AP2γ and BLIMP1 become expressed within fragilis$^+$ cells only when OTX2 has been turned off, suggesting that expression of OTX2 in fragilis$^+$ cells may prevent precocious activation of AP2γ and BLIMP1.

To determine whether these temporal changes in expression were mirrored *in vitro*, we analysed EpiLC-derived cell aggregates during PGCLC differentiation by using a modification of the established procedure (Hayashi et al., 2011) in which the concentrations of BMP4, BMP8A, SCF and EGF were reduced tenfold (protocol 1) as used previously (Zhang et al., 2018) (Fig. 1B). AP2γ$^+$ cells were first detected at day (d) 0.5; at d1 some AP2γ$^+$ cells co-expressed BLIMP1 and these increased in number up to d2; OCT4 was expressed in all cells up to d1 with expression remaining high in AP2γ$^+$ cells at d2; NANOG was activated at high levels predominantly in AP2γ$^+$-T$^-$ cells; and T showed widespread activation beginning at d1 prevalently in AP2γ$^-$ cells expressing low levels of NANOG (Fig. 1C). A comparison of OTX2 expression with that of OCT4, NANOG, AP2γ and T showed that, although markedly downregulated between d0 and d1 (Zhang et al., 2018) and virtually undetectable at d2 (Fig. 1C), OTX2 remained detectable at d0.5 and d1 in numerous cells co-expressing OCT4 and low levels of NANOG; from d1 T was also detectable (Fig. 1C). Notably, at d0.5, OTX2 was absent from AP2γ$^+$ cells. This analysis confirms and extends previous findings (Zhang et al., 2018) indicating that, during the germline and somatic differentiation time window, OTX2 is efficiently repressed in epiblast-derived or EpiLC-derived cells as they begin to differentiate towards PGCs or PGCLCs, while it is maintained for longer in somatic precursors. This suggests that differential OTX2 repression may prevent excessive germline differentiation.

OTX2 binding to *Nanog* or *Oct4* enhancer region regulates the generation of PGCLCs and somatic cells

To assess the hypothesis that differential OTX2 repression governs the extent of germline entry, we analysed ESCs in which specific OTX2 binding site(s) (Obs) were mutagenized. *Nanog*Δ*Obs3* ESCs have lost the strongest Obs (Obs3) in the *Nanog* enhancer (Acampora et al., 2016). In addition, we derived *Oct4*Δ*Obs* ESC lines mutagenized in the three Obs located in the enhancer region of *Oct4* (Fig. S1A-D): Obs1 within the PE, Obs2 at the 5′ of the PE and Obs3 at the 3′ of the DE (Fig. S2A). Compared with wild type, the OTX2-binding activity in *Oct4*Δ*Obs* ESCs and d2 EpiLCs was virtually abrogated (Fig. S2B). However, wild-type and *Oct4*Δ*Obs* ESCs showed no differences in: self-renewal at clonal density (Fig. S2C; Table S1); expression of OCT4, NANOG, OTX2 and OCT6 (also known as *Pou3f1*) (Fig. S2D); ability to convert into the naïve state (Fig. S2E); steady state LIF, FGF, WNT and BMP signaling (Fig. S2F); acute responsiveness to LIF (Fig. S2G) and FGF2 (Fig. S2H); and chimaera-forming capacity (Fig. S2I). Furthermore, analysis of *Oct4*Δ*Obs* and *Nanog*Δ*Obs3* EpiLCs at d2 showed uniform high level of OCT4, OTX2 and OCT6, absence of NANOG and T (Fig. S2J), and similar steady state levels of phospho (p)-ERK1,2, p-SMAD1,5,8, p-β-catenin, active β-catenin and p-SMAD2 (Fig. S2K). Together, these results indicate that *Oct4*Δ*Obs* ESCs and both *Oct4*Δ*Obs* and *Nanog*Δ*Obs3* EpiLCs are indistinguishable from wild-type cells.

To investigate whether *Oct4*Δ*Obs* and *Nanog*Δ*Obs3* (subsequently referred to as Δ*Obs*) ESCs are affected in their propensity to differentiate into germline cells, we employed the above-mentioned protocol 1 as a PGCLC differentiation method (Fig. 2A). FACS analysis (Fig. S3A-C) for SSEA1 (also known as *Fut4*) and CD61 (also known as *Itgb3*), which are co-expressed in PGCLCs, indicated that compared with wild type, Δ*Obs* mutants generated a higher percentage of SSEA1$^+$-CD61$^+$ cells at d6, approaching that of *Otx2* null (*Otx2KO*) cells (Zhang et al., 2018) (Fig. 2B). This finding was confirmed with independently generated Δ*Obs* cell lines (Fig. 2C). To determine whether increased generation of PGCLCs was presaged by altered expression of TFs, cytospin preparations of d2 cell aggregates were analysed. Relative to wild type, Δ*Obs* mutants showed an increased proportion of cells expressing high levels of OCT4, NANOG and BLIMP1, and a decreased proportion of T$^+$ cells (Fig. 2D; Fig. S3D,E; Table S2). Immunohistochemistry analysis of d2 cell aggregates supported cytospin data (Fig. 2E). Real-time quantitative PCR (RT-qPCR) analysis indicated that the expression levels of *Oct4*, *Nanog*, *Ap2γ* and *Blimp1* were also increased at d2 in mutants (Fig. 2F). For *Nanog* and *Blimp1* this was apparent at d0.5; for *Ap2γ* it was evident at d0.25 (Fig. 2F). No difference in *Otx2* expression was detected between wild type and Δ*Obs* mutants, whereas the expression levels of *T* and *Hoxb1* were substantially diminished in Δ*Obs* mutants and virtually extinguished in *Otx2KO* cells (Fig. 2F,G). Previous studies reported that histone H3 tri-methyl lysine 9 (H3K9me3) is enriched at poised enhancers and may distinguish poised and active states for the DE and PE of *Oct4* (Wu and Schöler, 2014). Compared with wild type, in *Oct4*Δ*Obs* d2 cell aggregates, the H3K9me3 level was reduced on the DE (Fig. 2H), suggesting a repressive role for OTX2 on DE activity. Increased generation of SSEA1$^+$-CD61$^+$ cells was observed in mutants also when PGCLC differentiation was initiated from ESCs maintained in serum plus LIF (protocol 2) (Fig. 2I,J; Fig. S4A). Therefore, in contrast to wild type and similar to *Otx2KO* cells, germline differentiation of Δ*Obs* mutants is increased at the expense of somatic fate.

Development (2021) 148, dev199166. doi:10.1242/dev.199166

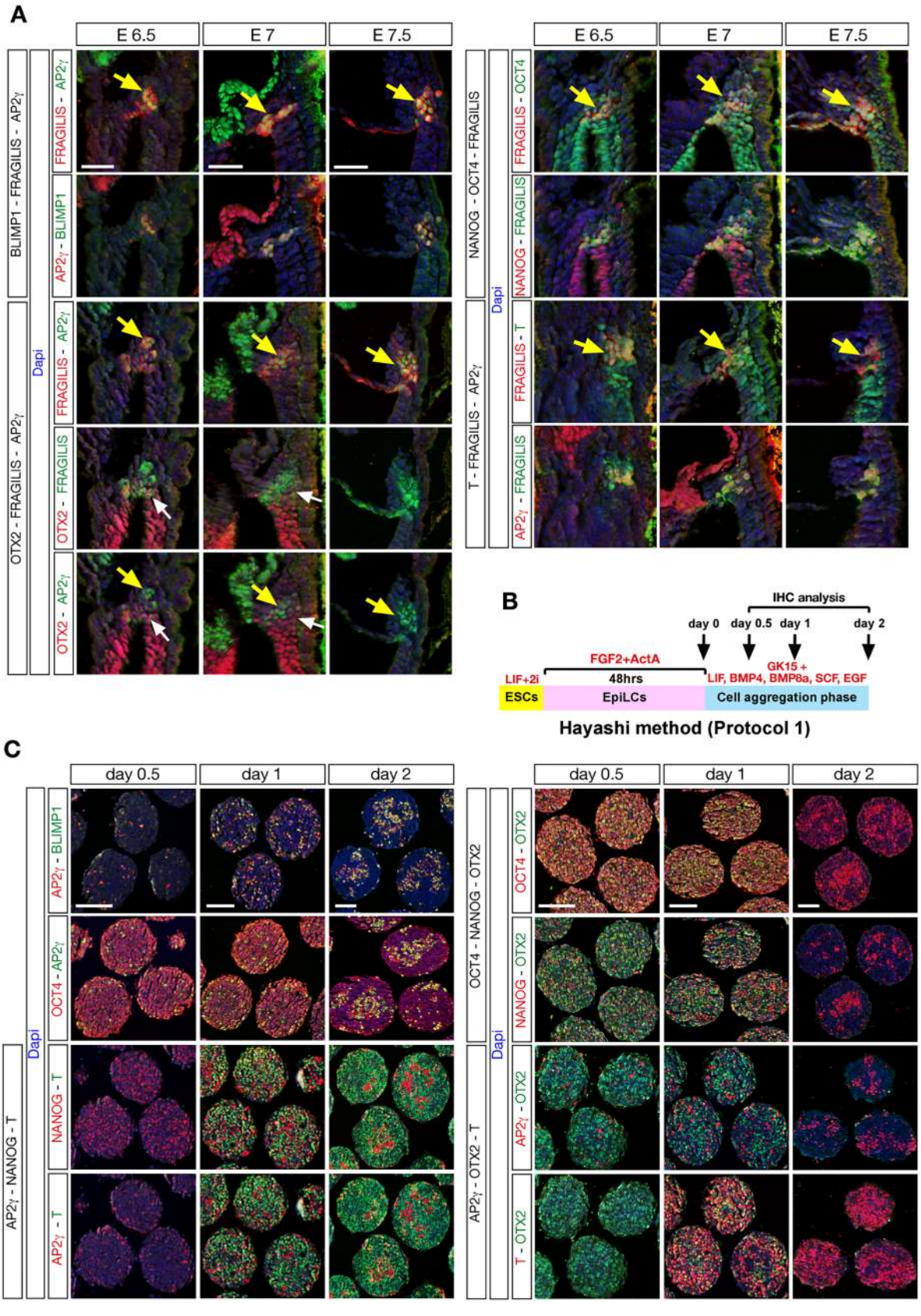

Fig. 1. Expression analysis during germline differentiation. (A) Representative sections of E6.5, E7 and E7.5 embryos stained with the indicated antibody combinations. Yellow arrows, differentiating PGCs; white arrows, fragilis^{+}-AP2γ^{-} cells with low or moderate OTX2 levels. At E6.5, sections are along a sagittal-oblique plane; at E7 and E7.5, sections are along a sagittal plane. Scale bars: 50 µm. (B) Protocol 1 experimental design. Cell aggregates were analysed at d0.5, d1 and d2. (C) Immunohistochemistry analysis performed on representative sections using the indicated antibody combinations. Scale bars: 100 µm (A,C). Sections are counterstained with DAPI.

Development (2021) 148, dev199166. doi:10.1242/dev.199166

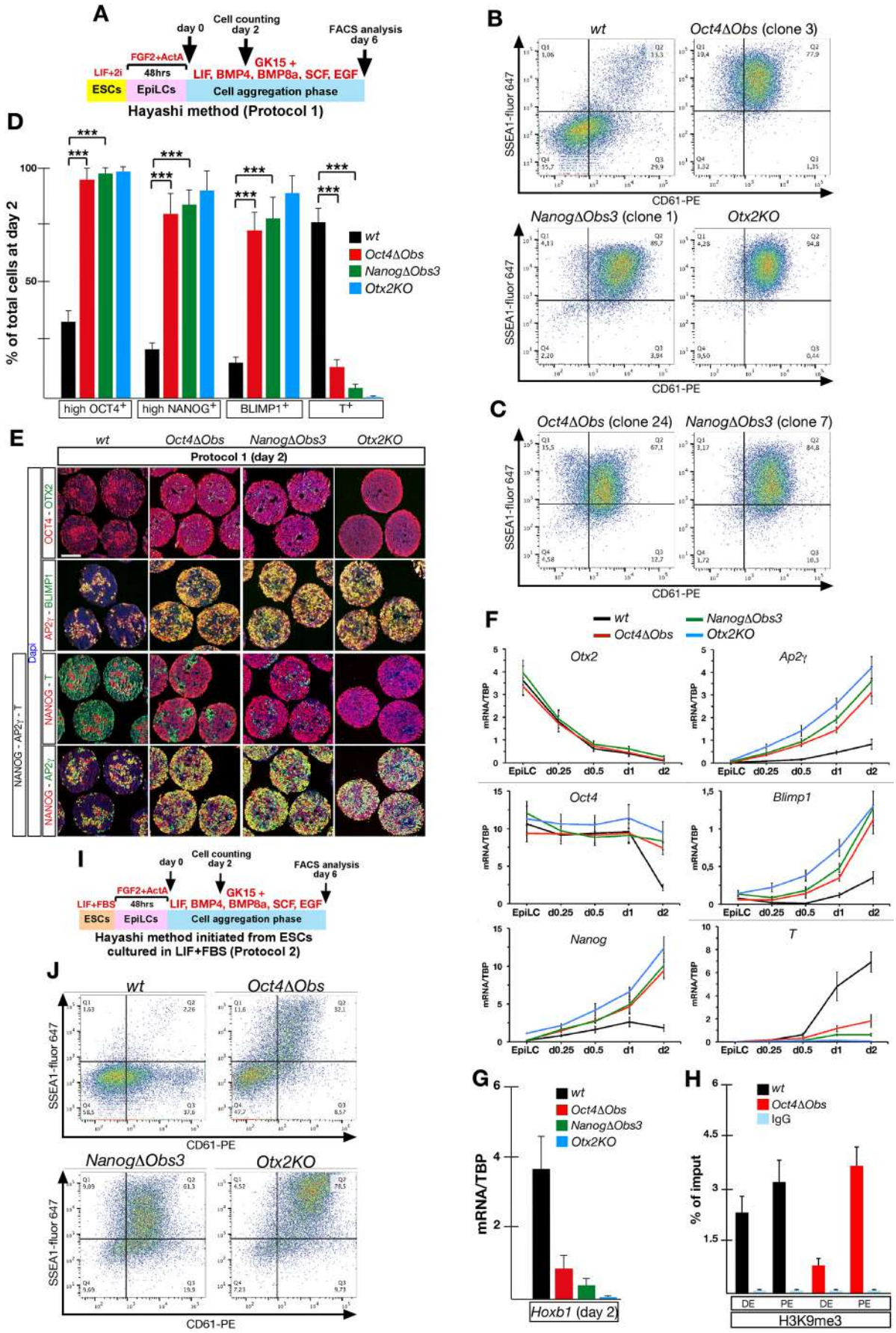

Fig. 2. See next page for legend.

Development (2021) 148, dev199166. doi:10.1242/dev.199166

Fig. 2. OTX2 binding to *Oct4* or *Nanog* enhancer region regulates PGCLC and somatic mesoderm differentiation. (A) Protocol 1 experimental design. (B,C) FACS analysis performed at d6 on wild-type, Δ*Obs* and *Otx2KO* cell aggregates with SSEA1 and CD61 antibodies. (D) Counting at d2 of cells expressing the indicated transcription factors in wild type and mutants. Data are mean±s.d. of three independent experiments. ***P<0.0005. (E) Representative immunostaining performed at d2 on sections from wild-type, Δ*Obs* and *Otx2KO* cell aggregates using the indicated antibodies. Sections are counterstained with DAPI. Scale bar: 100 µm. (F,G) RT-qPCR analysis showing the expression profile of *Otx2*, *Oct4*, *Nanog*, *Ap2γ*, *Blimp1* and *T* in EpiLCs and in cell aggregates at d0.25, d0.5, d1 and d2 (F), and *Hoxb1* expression at d2 (G). Data were normalized to *Tbp* mRNA and are reported as the mean±s.d. of three independent experiments. (H) ChIP-qPCR analysis performed at d2 in wild-type and *Oct4*Δ*Obs* cell aggregates to assess the H3K9me3 enrichment level on the DE and PE of *Oct4*. Data are mean±s.d. of three independent experiments. (I) Protocol 2 experimental design. (J) FACS analysis at d6 on wild-type, Δ*Obs* and *Otx2KO* cell aggregates with SSEA1 and CD61 antibodies.

Cytokine requirements for germline and somatic differentiation of Δ*Obs* mutants

Otx2KO EpiLCs can undergo germline entry in the absence of cytokines (Zhang et al., 2018). To determine whether Δ*Obs* EpiLCs possessed the same capacity, we employed a cytokine-free differentiation protocol (protocol 3) (Fig. 3A). FACS analysis at d6 revealed moderate generation of PGCLCs only in *Otx2KO* cells (Fig. 3B). Cell counting and immunohistochemistry experiments showed that at d2 Δ*Obs* mutants significantly increased the percentage of total cells expressing high OCT4 and high NANOG, and decreased the proportion of T^+ cells (Fig. 3C; Figs S3D,E and S4B; Table S2). The $BLIMP1^+$ cell fraction was expanded only in *Otx2KO* cells. RT-qPCR analysis showed that repression of *Otx2* was equally delayed in all genotypes, and that expression of *Nanog*, *Oct4*, *Ap2γ* , *Blimp1* and *T* at d2 was coherent with cell counting data (Fig. 3D). At earlier time points, the expression of these factors was similar in all genotypes except for *Blimp1* and *Ap2γ*, which were increased and precocious in *Otx2KO* cells (Zhang et al., 2018) (Fig. 3D). *Hoxb1* was inefficiently upregulated in mutants (Fig. 3E). Therefore, in the absence of cytokines, Δ*Obs* mutants, in contrast to *Otx2KO* cells, are unable to promote germline differentiation. This suggests that cytokine-independent germline differentiation of Δ*Obs* mutants may require OTX2 functions in addition to those depending on OTX2 binding to *Oct4* or *Nanog* enhancer region. LIF is required for proliferation and survival of germ cells (Hayashi et al., 2011; Farini et al., 2005; Koshimizu et al., 1996; Cheng et al., 1994) and to maintain pluripotency and promote self-renewal of ESCs (Matsuda et al., 1999; Niwa et al., 2009). As these functional properties may have an impact on germline differentiation of Δ*Obs* and *Otx2KO* mutants, we analysed cell aggregates cultured with LIF only (protocol 4) (Fig. 4A). Compared with wild type, Δ*Obs* and *Otx2KO* mutants generated more PGCLCs at d6 (Fig. 4B), and at d2 showed increased percentage of total cells expressing high OCT4, high NANOG and BLIMP1, and a virtual absence of T^+ cells (Fig. 4C; Figs S3D,E and S4C; Table S2). RT-qPCR analysis showed that *Otx2* was efficiently repressed in all genotypes (Fig. 4D), while, compared with wild type, *Oct4* expression was maintained at high levels in mutant cell aggregates, *Blimp1*, *Ap2γ* and *Nanog* expression was activated earlier, and *T* and *Hoxb1* expression was severely decreased (Fig. 4D,E). Therefore, LIF is sufficient to promote significant germline differentiation in Δ*Obs* mutants and, with a substantially higher efficiency, in *Otx2KO* cells.

To further investigate the contribution of LIF to PGCLC differentiation, we used a protocol in which LIF was the only component omitted from the cytokine cocktail (protocol 5) (Fig. 4F). Compared with wild type, the number of PGCLCs at d6 was increased in Δ*Obs* and *Otx2KO* mutants (Fig. 4G). At d2, the percentage of total cells expressing high OCT4, high NANOG and BLIMP1 was significantly increased in all mutants, while the number of T^+ cells was strongly affected only in *Otx2KO* cells (Fig. 4H; Figs S3D,E and S4D; Table S2). RT-qPCR analysis showed that repression of *Otx2* and activation of *Nanog*, *Blimp1* and *Ap2γ* were both less efficient than in protocols 1 and 4 (Fig. 4I). Compared with wild type, *T* and *Hoxb1* activation was weakened in mutants (Fig. 4I,J). Taken together, findings from protocols 4 and 5 indicate that LIF alone provides a more effective stimulation of PGCLC differentiation than the remaining cytokines, and is particularly effective in suppressing somatic fate.

Previous work showed that endogenous WNT activity contributes to *Otx2* repression in different contexts and can be mimicked by the glycogen synthase kinase 3 inhibitor (GSK3) CHIR99021 (CHIR) (Acampora et al., 2016; Neagu et al., 2020; Zhang et al., 2018). We therefore assessed whether CHIR alone may stimulate the generation of PGCLCs and somatic mesoderm (protocol 6) (Fig. 5A). Only *Otx2KO* cells produced a substantial proportion of $SSEA1^+$-$CD61^+$ cells at d6 (Fig. 5B). Compared with wild type and *Otx2KO* mutants, in Δ*Obs* mutants CHIR treatment generated intermediate percentages of cells expressing high OCT4, high NANOG and T (Fig. 5C; Figs S3D,E and S5A; Table S3), and intermediate expression levels of *Oct4*, *Nanog*, *T* and *Hoxb1* (Fig. 5D,E). However in wild type and Δ*Obs* mutants, the percentage of $BLIMP1^+$ cells and the expression levels of *Blimp1* and *Ap2γ* were both similar to those described in cytokine-free culture conditions (Fig. 5C,D). RT-qPCR analysis showed that *Otx2* repression was comparable with that observed in protocol 5 (Fig. 5D). These results reveal that stimulation of the WNT pathway induces robust PGCLC differentiation only in *Otx2KO* cells, while in Δ*Obs* and *Otx2KO* mutants it efficiently suppresses somatic differentiation.

LIF, WNT and BMP4 synergism promotes germline entry in Δ*Obs* mutants

To determine whether WNT stimulation may synergize with LIF signaling during PGCLC differentiation, as reported for ESCs (ten Berge et al., 2011; Karwacki-Neisius et al., 2013; Ogawa et al., 2006), we assessed the effects of simultaneous addition of LIF and CHIR (protocol 7) (Fig. 5F). Compared with wild type, the generation of PGCLCs at d6 was substantially higher in Δ*Obs* and *Otx2KO* mutants (Fig. 5G). This correlated with increased percentage of total cells expressing high OCT4, high NANOG and BLIMP1, severe decrease of T^+ cells (Fig. 5H; Figs S3D,E and S5B; Table S3), and precocious and robust expression of *Nanog*, *Blimp1* and *Ap2γ* (Fig. 5I). In addition, *T* and *Hoxb1* were not activated and *Otx2* was efficiently repressed (Fig. 5I,J). To explore whether low levels of stimulation of other pathways could likewise potentiate the effects of LIF, we assessed differentiation in the presence of LIF and a low dose of BMP4, BMP8a, SCF and EGF (protocol 8) (Fig. 6A), the concentrations of which were ten times lower than those used in protocols 1 and 5. Compared with wild type, Δ*Obs* and *Otx2KO* mutants showed that PGCLC generation at d6 (Fig. 6B) and the number of cells expressing high OCT4, high NANOG and BLIMP1 at d2 were both markedly increased, while the number of T^+ cells was considerably diminished (Fig. 6C; Figs S3D,E and S5C; Table S3). RT-qPCR assays showed expression profiles similar to those obtained with LIF plus CHIR (Fig. 5I,J). Compared with protocol 8, cell aggregates supplemented

Development (2021) 148, dev199166. doi:10.1242/dev.199166

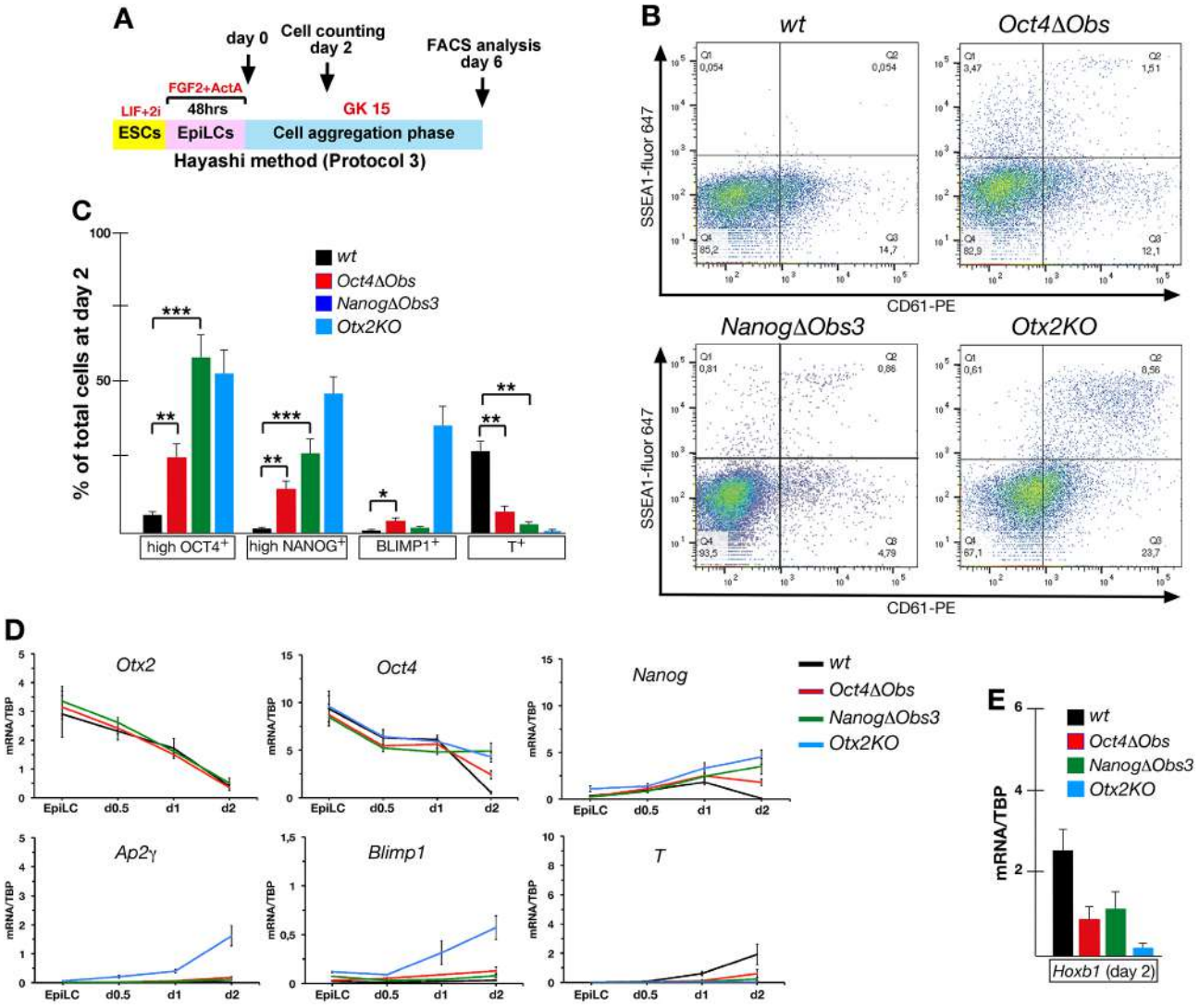

Fig. 3. Cytokine requirement for PGCLC differentiation in Δ*Obs* mutants. (A) Protocol 3 experimental design. (B) FACS analysis for SSEA1 and CD61 at d6 on wild-type, Δ*Obs* and *Otx2KO* cell aggregates. (C) Counting at d2 of cells expressing the indicated transcription factors in wild type and mutants. Data are mean±s.d. of three independent experiments. **P*=0.001-0.005, ***P*<0.001, ****P*<0.0005. (D,E) RT-qPCR analysis of the indicated transcripts at the time points shown (D) and *Hoxb1* expression at d2 (E). Data were normalized to *Tbp* mRNA and are reported as mean±s.d. of three independent experiments.

only with low concentrations of BMP4, BMP8A, SCF and EGF showed that the generation of SSEA1$^+$-CD61$^+$ cells was reduced in *Otx2KO* cells and virtually absent in Δ*Obs* mutants (Fig. S6A,B). Therefore, data from protocols 7 and 8 indicate that, in Δ*Obs* mutants, LIF addition to CHIR or to a minimal dose of BMP4, BMP8A, SCF and EGF promotes efficient germline entry and severely affects somatic lineage. Based on these results, we asked whether combining LIF with CHIR and low doses of BMP4, BMP8A, SCF and EGF (protocol 9) could further augment PGCLC differentiation (Fig. 6F). Interestingly, the number of PGCLCs (Fig. 6G), the percentage of total cells expressing high OCT4, high NANOG, BLIMP1 and T (Fig. 6H; Figs S3D,E and S5D; Table S3), and the expression profile exhibited by *Otx2*, *Oct4*, *Nanog*, *Ap2γ*, *Blimp1*, *T* and *Hoxb1* (Fig. 6I,J) were all similar to those obtained using protocol 1. Furthermore, the level of H3K9me3 detected in *Oct4*Δ*Obs* cells was decreased on the DE and increased on the PE (Fig. 6K), suggesting that, as shown for protocol 1, OTX2 is required to prevent transition of the DE status from a poised to an active condition. To further assess the similarities between mature PGCLCs generated by protocols 1 and 9, expression of PGCLC-specific mRNAs was examined by RT-qPCR. SSEA1$^+$-CD61$^+$ cells purified at d6 using protocols 1 and 9 showed very similar expression of 11 PGCLC-specific mRNAs in both wild-type and mutant PGCLCs (Fig. S6C). Therefore, in Δ*Obs* mutants, LIF, CHIR and low doses of BMP4, BMP8a, SCF and EGF may cooperatively induce high levels of PGCLCs counterbalanced by a severe decrease in somatic cells. Through this cooperation, Δ*Obs* mutants exhibit close similarity with *Otx2KO* cells, a finding previously reported only for protocol 1. The significance of these data was reinforced by a further control experiment showing that, in the presence of CHIR and low doses of BMP4, BMP8A, SCF and EGF, the generation of PGCLCs was considerably increased only in *Otx2KO* cells (Fig. S6D,E). To further investigate the role of LIF, the effect of titrating the LIF concentration on PGCLC differentiation was assessed. In GK15 media, the percentage of SSEA1$^+$-CD61$^+$ cells detected in wild-type cells was low but increased with increasing LIF concentrations, up to about 6% (Fig. S7A). In contrast, the mutant cell aggregates showed an

Development (2021) 148, dev199166. doi:10.1242/dev.199166

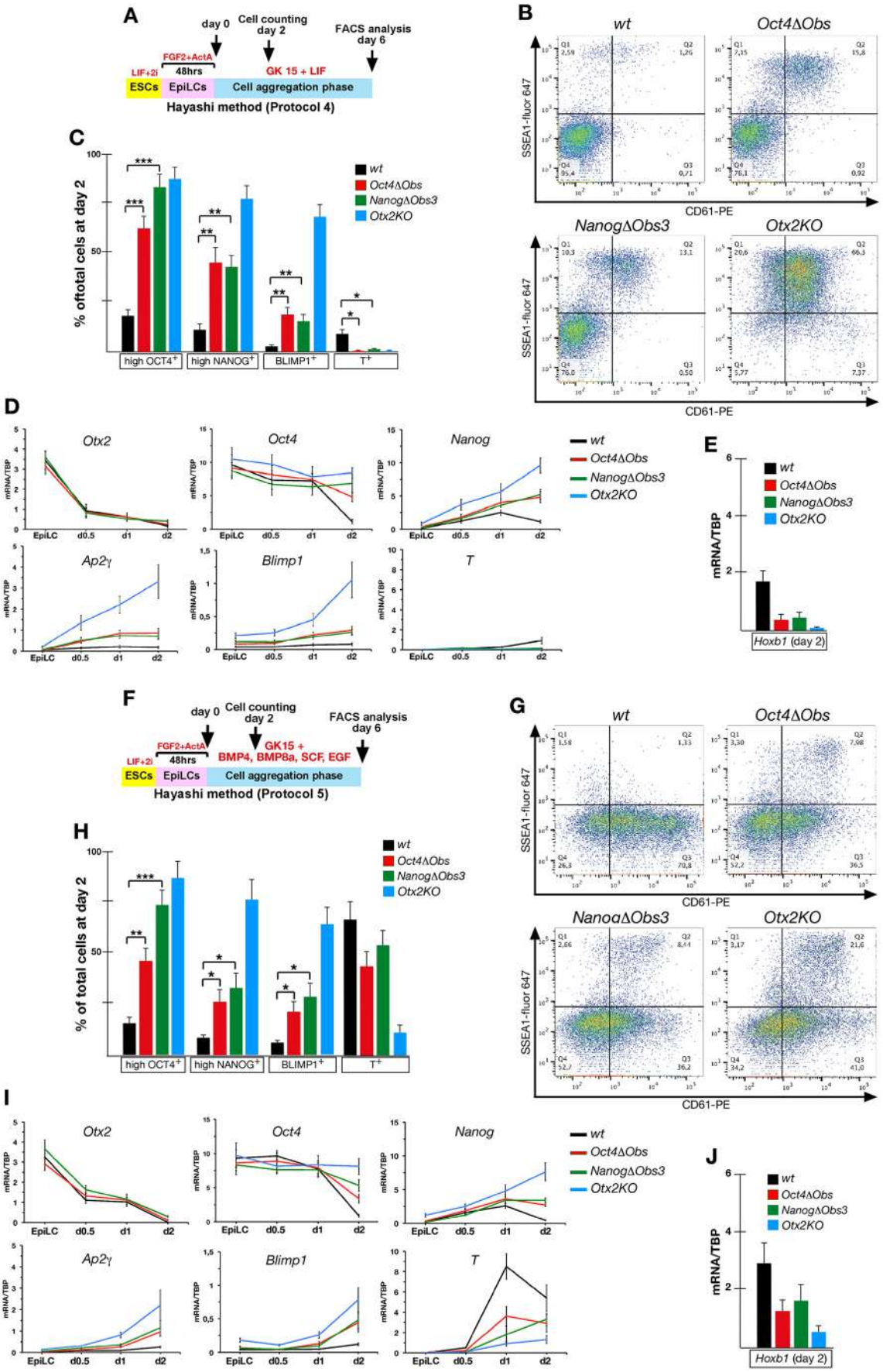

Fig. 4. See next page for legend.

Development (2021) 148, dev199166. doi:10.1242/dev.199166

Fig. 4. In Δ*Obs* mutants, LIF stimulates PGCLC differentiation and suppresses somatic fate more efficiently than BMP4. (A) Protocol 4 experimental design. (B) FACS analysis for SSEA1 and CD61 at d6 on wild-type, Δ*Obs* and *Otx2KO* cell aggregates. (C) Counting at d2 of cells expressing the indicated transcription factors in wild type and mutants. (D,E) RT-qPCR analysis of the indicated transcripts at the time points shown (D) and *Hoxb1* expression at d2 (E). (F) Protocol 5 experimental design. (G) FACS analysis for SSEA1 and CD61 at d6 on wild-type, Δ*Obs* and *Otx2KO* cell aggregates. (H) Counting at d2 of cells expressing the indicated transcription factors in wild type and mutants. (I,J) RT-qPCR analysis of the indicated transcripts at the time points shown (I) and *Hoxb1* expression at d2 (J). (C,H) Data are mean±s.d. of three independent experiments. **P*=0.001-0.005, ***P*<0.001, ****P*<0.0005. (D,E,I,J) Data were normalized to *Tbp* mRNA and are reported as the mean±s.d. of three independent experiments.

increased yield of SSEA1$^+$-CD61$^+$ cells at 1000 U/ml LIF, compared with 300 U/ml, but this was not further increased by raising the LIF concentration to 3000 U/ml (protocol 4) (Fig. S7B). When a similar LIF titration was performed using the fixed concentrations of CHIR and low doses of BMP4, BMP8A, SCF and EGF (protocol 9; Fig. S7C), a similarly patterned response was observed in both wild-type cells and in all mutant cell lines (Fig. S7D). Although the absolute proportions of SSEA1$^+$-CD61$^+$ cells was increased in each cell line, a saturating response to 1000 U/ml LIF was seen in all the mutants but not in the wild-type cells (Fig. S7B), which increased the percentage of PGCLCs up to 11% in response to 3000 U/ml of LIF.

Temporal expression changes during early PGCLC differentiation of Δ*Obs* mutants

Previous data showed that the OTX2 repressive control of *Oct4* and *Nanog* expression defines commitment of EpiLC-derived cells to germline or somatic lineage. To investigate this in greater depth, we analysed the combined expression of OTX2, OCT4, NANOG, SOX2, AP2γ and T in wild-type and Δ*Obs* cell aggregates at d0.5 and d1 using protocol 1. OCT4 and SOX2 were uniformly co-expressed in wild-type and Δ*Obs* cells, while NANOG was detected mostly at low level in wild type and at high level in Δ*Obs* cells (Fig. S8). Although, compared with EpiLCs, the *Otx2* mRNA was downregulated at d0.5 and d1 (Fig. 2F), OTX2 was detectable in numerous cells co-expressing OCT4 and low NANOG in wild-type aggregates but co-expressing OCT4 and prevalently high NANOG in Δ*Obs* mutants (Fig. S8). All NANOG$^+$ cells co-expressed SOX2 (Fig. S8). In wild-type cells at d0.5, AP2γ was detected in very few OTX2$^-$ cells co-expressing high NANOG, whereas in Δ*Obs* mutants, AP2γ was activated in a higher number of cells all co-expressing high NANOG and, frequently, also OTX2 (Fig. S8), suggesting that, in Δ*Obs* mutants, numerous OTX2$^+$ cells are permissive for AP2γ activation. However, by d1, AP2γ co-expression with OTX2 was lost, likely because of further downregulation of OTX2 in AP2γ$^+$ cells. Analysis of T showed that at d1 in wild-type cells, most of the OTX2$^+$ cells co-expressed T and low NANOG, while in Δ*Obs* mutants the few T$^+$ cells co-expressed only low NANOG (Fig. S8). These data suggest that OTX2-dependent widespread activation of the pluripotency GRN determines, in mutants, a precocious and extensive recruitment of EpiLC-derived cells for germline entry rather than for somatic fate.

The Obs2 in the *Oct4* enhancer plays a major role in germline and somatic differentiation

To determine which Obs in the *Oct4* enhancer is functionally relevant, we restored the wild-type sequence of Obs2, which exhibited the highest OTX2 binding activity, in the *Oct4*Δ*Obs* mutant and generated the *Oct4*Δ*Obs1,3* ESC line (Fig. S1E,F). ChIP analysis showed the expected recovery in OTX2 binding specifically at Obs2 (Fig. S9A,B). FACS analysis showed that the percentage of PGCLCs generated by using protocol 1 was similar in wild type and *Oct4*Δ*Obs1,3* mutant (Fig. S9C). Immunohistochemistry and cell counting at d2 (Figs S9D,E and S3D,E; Table S2) confirmed the similarity of *Oct4*Δ*Obs1,3* to wild-type cells, suggesting that OTX2 binding to Obs2 modulates the OCT4 requirement for germline and somatic differentiation.

Enforced OTX2 expression inefficiently suppresses germline entry in Δ*Obs* mutants

Previous work has shown that tamoxifen (Tx)-mediated nuclear translocation of OTX2-ER^{T2} fusion protein in wild-type and *Otx2KO* cells suppresses PGCLC differentiation (Zhang et al., 2018). We reasoned that, in contrast to wild-type and *Otx2KO* cells, nuclear translocation of OTX2-ER^{T2} in Δ*Obs* mutants should not affect functions depending on OTX2 binding to *Oct4* or *Nanog* enhancer region. To test this hypothesis, we generated *E14;Otx2ER^{T2}*, *Oct4*Δ*Obs;Otx2ER^{T2}*, *Nanog*Δ*Obs3;Otx2ER^{T2}* and *Otx2KO;Otx2ER^{T2}* ESC lines expressing a similar level of OTX2-ER^{T2} (Fig. S1G,H). In these cell lines, Tx exposure for 1 h induced efficient OTX2-ER^{T2} nuclear translocation (Fig. S1I). Two independent clones for *Oct4*Δ*Obs;Otx2ER^{T2}* and *Nanog*Δ*Obs3;Otx2-ER^{T2}* mutants were compared with *E14;Otx2ER^{T2}* and *Otx2KO;Otx2ER^{T2}* cell lines using protocol 1. Without Tx, the generation of PGCLCs was similar to that of the same parental cell lines (Fig. 7A). In Tx-treated cell aggregates (from d0 to d2 of the cell aggregation phase), the generation of PGCLCs was suppressed in *E14;Otx2ER^{T2}* and *Otx2KO;Otx2ER^{T2}* cell lines, severely affected in *Oct4*Δ*Obs;Otx2ER^{T2}* cells, but only partially impaired in *Nanog*Δ*Obs3;Otx2ER^{T2}* cells (Fig. 7B). Consistent with these findings, in Tx-treated d2 cell aggregates the generation of AP2γ$^+$-BLIMP1$^+$ cells was virtually abolished in *E14;Otx2ER^{T2}* and *Otx2KO;Otx2ER^{T2}* cells, decreased in *Oct4*Δ*Obs;Otx2ER^{T2}* cells, but less affected in *Nanog*Δ*Obs3;Otx2ER^{T2}* cell aggregates (Fig. 7C). Conversely, the generation of T$^+$ cells was severely impaired only in *Nanog*Δ*Obs3;Otx2ER^{T2}* cells (Fig. 7C). Interestingly, in *E14;Otx2ER^{T2}*, *Otx2KO;Otx2ER^{T2}* and *Oct4*Δ*Obs;Otx2ER^{T2}* cell lines, OCT4 expression was low in all cells including those AP2γ$^+$ (Fig. 7C), which did not activate NANOG and SOX2 (yellow and white arrows in Fig. 7C). In contrast, in the *Nanog*Δ*Obs3;Otx2ER^{T2}* mutant, a large fraction of AP2γ$^+$ cells showed high expression of OCT4 (pink arrows in Fig. 7C), NANOG and SOX2 (Fig. 7C). These data suggest that OTX2 binding to the *Nanog* enhancer is required to efficiently suppress germline differentiation and induce somatic fate. To investigate the possibility that OTX2 may repress germline determinants, we analysed whether BLIMP1$^+$ cells co-expressed nuclear OTX2-ER^{T2}. BLIMP1 and OTX2-ER^{T2} were colocalized in Tx-treated cells of all genotypes (Fig. 7D), which, in turn, also co-expressed AP2γ (Fig. 7C). In addition, we found that levels of *Prdm14* and *Blimp1* mRNAs, which are restricted to PGCLCs, showed a similar expression pattern in all cell lines (Fig. 7E). These data suggest that OTX2 does not directly repress *Blimp1*, *Ap2γ* and *Prdm14* during germline differentiation.

Δ*Obs* embryos generate supernumerary PGCs

To determine whether PGC development was affected also *in vivo*, we analysed Δ*Obs* homozygous embryos. Immunohistochemistry analysis of Δ*Obs* homozygous embryos at E6.7 and E7.5 revealed that expression of BLIMP1, AP2γ, fragilis, NANOG, OCT4, T and

Development (2021) 148, dev199166. doi:10.1242/dev.199166

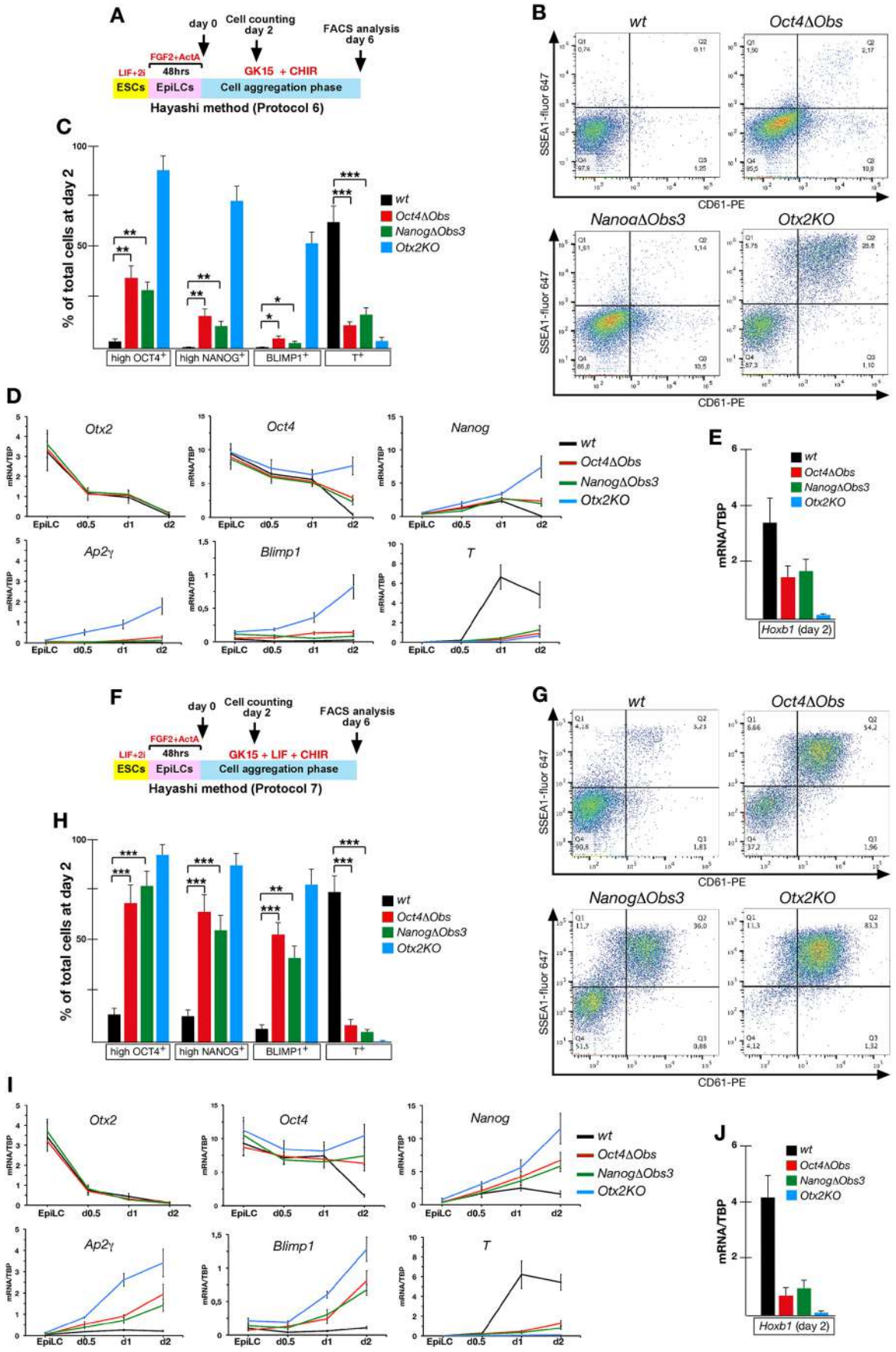

Fig. 5. See next page for legend.

Development (2021) 148, dev199166. doi:10.1242/dev.199166

Fig. 5. Germline entry of Δ*Obs* mutants is enhanced by LIF in conjunction with CHIR. (A) Protocol 6 experimental design. (B) FACS analysis for SSEA1 and CD61 at d6 on wild-type, Δ*Obs* and *Otx2KO* cell aggregates. (C) Counting at d2 of cells expressing the indicated transcription factors in wild type and mutants. (D,E) RT-qPCR analysis of the indicated transcripts at the time points shown (D) and *Hoxb1* expression at d2 (E). (F) Protocol 7 experimental design. (G) FACS analysis for SSEA1 and CD61 at d6 on wild-type, Δ*Obs* and *Otx2KO* cell aggregates. (H) Counting at d2 of cells expressing the indicated transcription factors in wild type and mutants. (I,J) RT-qPCR analysis of the indicated transcripts at the time points shown (I) and *Hoxb1* expression at d2 (J). (C,H) Data are the mean±s.d. of three independent experiments. **P*=0.001-0.005, ***P*<0.001 and ****P*<0.0005. (D,E,I,J) Data were normalized to *Tbp* mRNA and are reported as the mean±s.d. of three independent experiments.

OTX2 was similar to wild type (Fig. 8A). To determine the number of BLIMP1$^+$-fragilis$^+$ PGCs, we analysed wild-type and Δ*Obs* embryos at E7.5 and E8.5. All sections, including BLIMP1$^+$-fragilis$^+$ PGCs were captured for cell counting (Fig. S10). Compared with wild type, Δ*Obs* mutants exhibited about 1.5 times more PGCs at both E7.5 and E8.5 (Fig. 8B; Table S4). Ectopic PGCs were not identified. Therefore, binding of OTX2 to the *Oct4* or *Nanog* enhancer region is required to limit the extent of germline differentiation *in vivo*.

DISCUSSION

Differentiation of the epiblast into germline and somatic cells both *in vivo* and *in vitro* requires the action of BMP4, but the interplay with other signals, particularly WNT3, is also notable (Lawson et al., 1999; Saitou and Yamaji, 2012; Günesdogan and Surani, 2016; Aramaki et al., 2013). Previous studies have reported that LIF is required to sustain proliferation and survival of germ cells (Farini et al., 2005; Koshimizu et al., 1996; Cheng et al., 1994). The initial transition of epiblast-derived cells into the germline-competent state requires dismantling of the formative pluripotency GRN, characterized by high *Otx2* expression and PE-driven expression of *Oct4*, alongside activation of the PGC pluripotency GRN, characterized by extinction of *Otx2*, re-expression of *Nanog*, high *Sox2* expression and DE-driven expression of *Oct4* (Zhang and Chambers, 2019; Smith, 2017; Choi et al., 2016). Conversely, somatic differentiation requires transition of formative pluripotency into a primed state characterized by cell heterogeneity in expression of pluripotency TFs, including OTX2, NANOG and SOX2, as well as somatic gene expression.

Recent work has revealed that, in a germline permissive environment, downregulation of *Otx2* determines the number of epiblast-derived cells entering the germline differentiation program (Zhang et al., 2018; Zhang and Chambers, 2019; Laird, 2018). Nevertheless, the mechanisms by which OTX2 regulates the contribution of epiblast cells to germline and somatic lineage are unknown. As OTX2 binds to regulatory regions of *Oct4* and *Nanog* in EpiLCs (Acampora et al., 2016), we hypothesized that germline entry may require release of OTX2 repression on the PGCLC pluripotency GRN. Our data indicate that, through this binding, OTX2 influences germline and somatic fate choice of EpiLC-derived cells in response to LIF and high doses of BMP4, BMP8A, EGF and SCF. Indeed, Δ*Obs* and *Otx2KO* cell aggregates exhibit comparable phenotypes in terms of widespread activation of the pluripotency GRN, increased generation of PGCLCs and suppression of somatic fate. However, Δ*Obs* and *Otx2KO* mutants do not share all aspects of their phenotype in all protocols. Importantly, without cytokines, Δ*Obs* mutants, unlike *Otx2KO* cells (Zhang et al., 2018), do not generate PGCLCs. This suggests that OTX2 blocks cytokine-independent germline differentiation through functions other than those operating via binding to *Oct4* or *Nanog*. Such additional OTX2 functions could involve repression of PGCLC TFs. However, our evidence suggests that OTX2 does not directly repress *Blimp1*, *Prdm14* and *Ap2γ*.

To determine the signaling pathway modulations that may provide equally efficient PGCLC differentiation in Δ*Obs* and *Otx2KO* mutants, we analysed the effects of LIF, WNT or BMP4 alone (protocols 4-6). None of these protocols raises the efficiency of PGCLC generation by Δ*Obs* cells to the level achieved in *Otx2KO* mutants. However, the combined action of LIF, CHIR and a low dose of BMP4, BMP8A, EGF and SCF suppresses the OTX2 functions that hamper Δ*Obs* mutants from highly efficient, *Otx2KO*-like, germline entry to the same extent as in culture conditions with LIF and high doses of BMP4, BMP8A, EGF and SCF. These data suggest that the generation of germ cells may be quantitatively correlated to specific combinations of cytokines whose inducing efficiency may also be influenced by the genetic state of the responding cells. In this context it would be interesting to assess whether, in embryos, the proximal-posterior epiblast includes restricted subdomains where identity and fate of epiblast-derived cells are precisely regulated by different concentrations of LIF, BMP and WNT signaling molecules.

Together with dose-dependent experiments (Fig. S7), our data indicate that LIF has an important role in PGCLC differentiation. We suggest that LIF signaling may improve the generation of PGCLCs by enhancing the proliferation/self-renewal of those cells that have released OTX2-dependent suppression of the pluripotency GRN. This interpretation may explain the beneficial effect of LIF on the generation of PGCLCs in all protocols where it is included, and, in addition, supports the similarity with ESCs where LIF is required to maintain pluripotency and self-renewal (Matsuda et al., 1999; Niwa et al., 2009), even through synergism with WNT and BMP4 signaling (ten Berge et al., 2011; Karwacki-Neisius et al., 2013; Ogawa et al., 2006; Ying et al., 2003, 2008). Notably, as *Otx2KO* ESCs can self-renew in the absence of LIF (Acampora et al., 2013), this might explain the propensity of *Otx2KO* ESCs to enter the germline in the absence of LIF. We propose that, in wild-type cells, LIF, BMP4 and WNT cooperate to repress *Otx2* early during the cell aggregation phase (Fig. 9). This generates two types of EpiLC-derived cells: those lacking OTX2 (OTX2$^-$) (right in Fig. 9A) and those transiently retaining OTX2 (OTX2$^+$) (left in Fig. 9A). OTX2$^-$ cells cannot repress the PGCLC pluripotency GRN; they enter the unipotent germline state, are expanded by LIF or LIF in synergism with BMP4 and/or WNT, and differentiate into PGCLCs (right in Fig. 9A). Conversely, OTX2-mediated repression of the PGCLC pluripotency GRN in OTX2$^+$ cells promotes entry into primed pluripotency and activation of somatic determinants leading to differentiation into somatic mesoderm (left in Fig. 9A). Our data do not exclude the possibility that BMP4 and WNT may also facilitate activation of somatic mesoderm genes (left in Fig. 9A). In Δ*Obs* mutants (Fig. 9B), *Otx2* repression by LIF, BMP4 and WNT, and generation of OTX2$^-$ (right in Fig. 9B) and OTX2$^+$ (left in Fig. 9B) EpiLC-derived subtypes is comparable with wild-type cells. In Δ*Obs* mutants, the OTX2$^-$ EpiLC-derived cell fraction corresponds to the wild-type OTX2$^-$ cell fraction, is naturally competent for germline differentiation and is unaffected by loss of OTX2 binding to *Oct4* or *Nanog* enhancer region (right in Fig. 9A,B). However, in the OTX2$^+$ cell fraction, progression towards the somatic fate is impaired by the inability of OTX2 to repress the pluripotency GRN

Development (2021) 148, dev199166. doi:10.1242/dev.199166

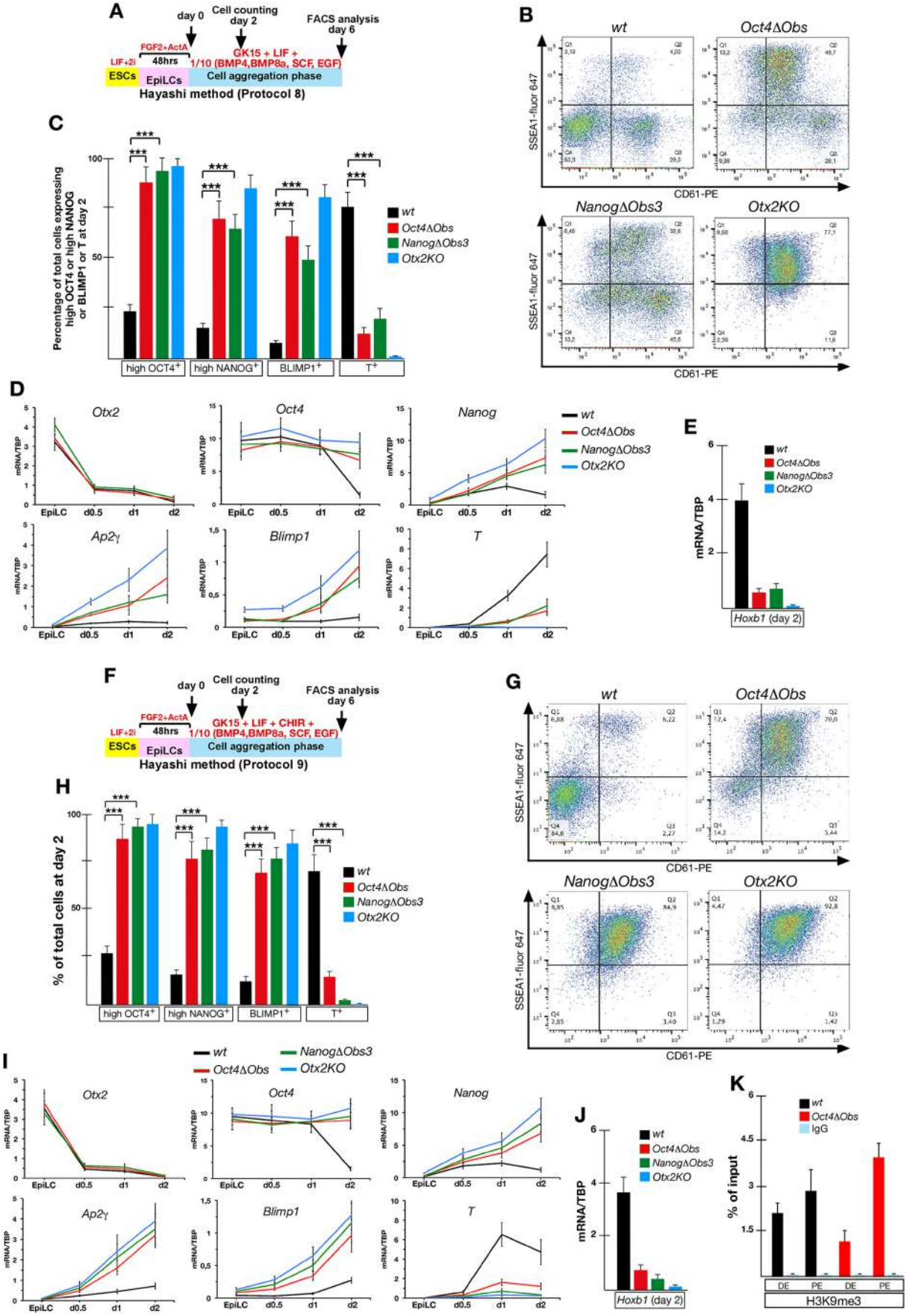

Fig. 6. See next page for legend.

Development (2021) 148, dev199166. doi:10.1242/dev.199166

Fig. 6. Germline entry of Δ*Obs* mutants is markedly increased by LIF in synergism with CHIR and low doses of BMP4, BMP8A, SCF and EGF. (A) Protocol 8 experimental design. (B) FACS analysis for SSEA1 and CD61 at d6 on wild-type, Δ*Obs* and *Otx2KO* cell aggregates. (C) Counting at d2 of cells expressing the indicated transcription factors in wild type and mutants. (D,E) RT-qPCR analysis of the indicated transcripts at the time points shown (D) and *Hoxb1* expression at d2 (E). (F) Protocol 9 experimental design. (G) FACS analysis for SSEA1 and CD61 at d6 on wild-type, Δ*Obs* and *Otx2KO* cell aggregates. (H) Counting at d2 of cells expressing the indicated transcription factors in wild type and mutants. (I,J) RT-qPCR analysis of the indicated transcripts at the time points shown (I) and *Hoxb1* wild type at d2 (J). (K) ChIP-qPCR analysis performed at d2 in wild-type and *Oct4*Δ*Obs* cell aggregates to assess the H3K9me3 enrichment level on the DE and PE of *Oct4*. Data are mean±s.d. of three independent experiments. (C,H) Data are mean±s.d. of three independent experiments. ***P<0.0005. (D,E,I,J) Data were normalized to *Tbp* mRNA and are reported as the mean±s.d. of three independent experiments.

(left in Fig. 9B). Consequently, cells that activate the pluripotency GRN may be further expanded by cytokines and commit to germline entry. These early events result in an increased recruitment of EpiLC-derived cells for germline entry before somatic differentiation is initiated with a consequent switch from somatic to germline fate (Fig. 9B). According to this model, nuclear translocation of OTX2-ER^{T2} can revert the germline to somatic fate switch in all cell lines except *Nanog*Δ*Obs3;Otx2ER*^{T2} cells (Zhang et al., 2018), indicating that OTX2 binding to the *Nanog* enhancer region efficiently suppresses the PGCLC pluripotency GRN. Interestingly, compared with *Oct4*Δ*Obs;Otx2ER*^{T2} cells, *Nanog*Δ*Obs3;Otx2ER*^{T2} mutants produced a higher proportion of presumptive PGCLCs in the presence of Tx, indicating that OTX2 suppression of *Nanog* transcription may play a greater role in preventing PGCLC differentiation than suppression of *Oct4* transcription. A possible explanation may reside in the expression baseline exhibited by *Nanog* and *Oct4* in EpiLCs. Indeed for *Nanog*, transition from the EpiLC state to the cell-aggregation phase is accompanied by re-activation from a silent state; for *Oct4* this transition does not involve activation of expression, which is similar in EpiLCs and in early EpiLC-derived cell aggregates, but a change in its expression control from the PE to DE. Moreover, only in Tx-treated *Nanog*Δ*Obs3;Otx2ER*^{T2} cells is activation of *Nanog* accompanied by induction of *Sox2* in presumptive PGLCs, suggesting that NANOG is required to induce *Sox2* and that both of them activate DE-driven expression of *Oct4* when OTX2 is suppressed. Notably, NANOG and SOX2 have been reported to bind to the DE of *Oct4* (Wu and Schöler, 2014).

Importantly, this study shows that the repressive control exerted by OTX2 on *Oct4* or *Nanog* also occurs in Δ*Obs* homozygous embryos, which exhibit increased numbers of PGCs. Notably, PGC generation is not detected at ectopic sites in mutant embryos. This suggests that only proximal-posterior epiblast-derived cells, which lie close to the BMP4 source in the extra-embryonic ectoderm, respond to loss of OTX2 binding to the *Oct4* or *Nanog* enhancer region by expanding generation of PGCs. However, our data do not currently distinguish between mechanisms involving a somatic mesoderm to germline fate switch of epiblast-derived cells or an alternative, cell-autonomous preferential proliferation of PGC precursors. In sum, previous work identified *Otx2* as a crucial determinant controlling allocation of epiblast cells to germline or somatic lineage (Zhang et al., 2018). Here we show that repression of *Oct4* and *Nanog* is a major mechanism by which OTX2 balances the contribution of epiblast cells to germline and somatic lineage, and, in addition, that OTX2 plays further roles preventing germline entry in the absence of cytokines.

MATERIALS AND METHODS

Generation of ESC and mouse mutants

Mutant ESC lines were generated by homologous recombination into E14Tg2a cells. The *Nanog*Δ*Obs3* ESC lines corresponding to clones 1 and 7, have previously been described (Acampora et al., 2016). In this study, clone 1 was used for all experiments and clone 7 for independent confirmatory assays (Fig. 2). As for the *Oct4*Δ*Obs* ESC line, the mutant version of Obs1, Obs2 or Obs3 (Fig. S1A) was first introduced in the 5′ flanking sequence of the *Oct4* gene by PCR-mediated mutagenesis; this region was then inserted into the targeting vector. Correct targeting into ESCs was assessed by Southern blot with probe a (Fig. S1B,C). Two *Oct4*Δ*Obs-neo/+* ESC clones were subjected to alternate rounds of neomycin cassette removal and re-targeting to obtain two independent homozygous ESC lines corresponding to clones 3 and 24, as confirmed by Southern blot and PCR analysis (Fig. S1C,D). Clone 24 represented an independent clone for confirmatory experiments (Fig. 2). The *Oct4*Δ*Obs* clone 3 was employed to perform all the experiments reported in this study. The *Oct4*Δ*Obs/+* ESC clone used to generate the *Oct4*Δ*Obs* clone 3, was also injected into C57BL/6 blastocysts to establish a mouse colony, which was kept in the B6D2 genetic background. *Oct4*Δ*Obs* homozygous mice were healthy and fertile. The homozygous *Oct4*Δ*Obs1,3* ESC line was also obtained by two alternate rounds of targeting and neomycin cassette removal in the homozygous *Oct4*Δ*Obs* cell line, by using a targeting vector carrying the mutant version of Obs1 and Obs3 sequences, but with the Obs2 sequence reverted to that of the wild-type gene (Fig. S1E). Genotyping of the homozygous *Oct4*Δ*Obs1,3* cells was confirmed by PCR with allele-specific primers (Fig. S1F) and Southern blot (not shown). Primers for genotyping are listed in Table S5. The *pPyCAGOtx2-ER*^{T2} plasmid (Zhang et al., 2018) (Fig. S1G) was electroporated into E14 *Nanog*Δ*Obs3*, *Oct4*Δ*Obs* and *Otx2KO* ESCs to generate cell lines showing cytoplasmic and ubiquitous distribution of the *OTX2-ER*^{T2} fusion protein, the nuclear translocation of which was dependent on 4-hydroxytamoxifen (Tx) (Sigma) administration. Twelve randomly integrated clones for each mutant cell line were assayed by western blot to determine transgene expression. ESC lines exhibiting comparable levels of OTX2-ER^{T2} were identified and those showing a level approximately twice that exhibited by the endogenous OTX2 were selected (Fig. S1H). These clones were then assayed by immunostaining with an antibody directed against ER. In the absence of Tx, the OTX2-ER^{T2} protein was prevalently localized to the cytoplasm, whereas 1 h of Tx (200 nM) exposure was sufficient to confine OTX2-ER^{T2} to the nucleus (Fig. S1I).

All ESC lines of this study tested negative for mycoplasma contamination. Experiments involving the use of animals were carried out in accordance under authorization 1196/2015-PR from the Italian Ministry of Health.

Cell culture experiments

ESCs were either cultured in Glasgow Minimum Essential Medium (GMEM) (Sigma) supplemented with 12% FBS (HyClone) and 1000 U/ml of leukaemia inhibitory factor (LIF) (Millipore) (referred to as FBS+LIF), or in serum-free N2B27 medium (Gibco) supplemented with 500 U/ml LIF, 1 µM of the mitogen-activated protein kinase kinase 1/2 (MEK1/2) inhibitor PD325901 (PD) and 3 µM of the glycogen synthase kinase 3 (GSK3) inhibitor CHIR99021 (CHIR) small molecules (both from Calbiochem) (referred to as LIF+2i) (Ying et al., 2008). Cell aggregates were generated from EpiLCs induced from ESCs adapted to LIF+2i medium for a minimum of seven passages or maintained in FBS+LIF. ESCs (2×10^5) were cultured in a six-well plate coated with human fibronectin (Sigma) (16.7 µg/ml) in serum-free N2B27 medium containing 1% KnockOut Serum Replacement (KSR, Gibco ThermoFisher), 12 ng/ml of basic fibroblast growth factor (FGF2) (PeproTech) and 20 ng/ml activin A (R&D Systems) for 48 h (Buecker et al., 2014). EpiLCs were then dissociated with TrypLE reagents (Gibco ThermoFisher) and resuspended at a concentration of 8×10^4 cells/ml in GMEM medium containing 15% KSR (GK15) or together with various combinations of cytokines and small molecules. Next, 25 µl of cell suspension (about 2000 cells) was plated on the lids of tissue culture dishes and incubated, as hanging drops, over PBS-containing bottom plates. After 2 days, cell aggregates were either collected for immunohistochemistry on

Development (2021) 148, dev199166. doi:10.1242/dev.199166

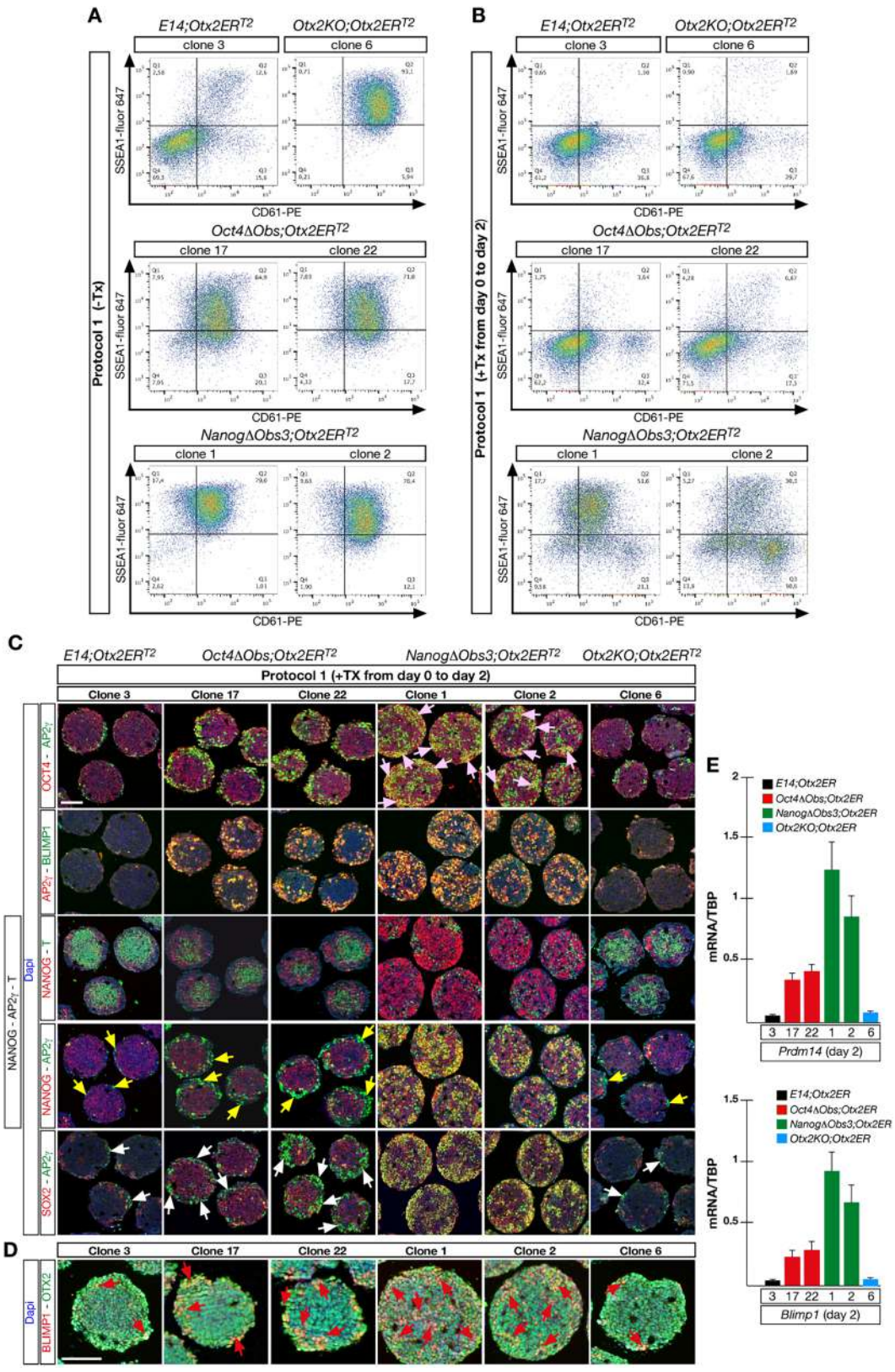

Fig. 7. Nuclear translocation of *OTX2-ER^{T2}* attenuates without suppressing germline entry of *Oct4ΔObs* and *NanogΔObs3* cell lines. (A,B) FACS analysis for SSEA1 and CD61 at d6 on the indicated mutant cell lines cultured according to protocol 1 with (A) or without (B) Tx from d0 to d2. (C) Immunohistochemistry experiments performed at d2 on representative sections from Tx-treated cell lines stained with the indicated antibodies. AP2γ^{+} PGCLCs co-express high NANOG (yellow arrows), SOX2 (white arrows) and high OCT4 (pink arrows) only in *NanogΔObs3;Otx2ER^{T2}* cells. (D) Immunostaining assays showing that OTX2-ER^{T2} is co-expressed with BLIMP1 in all cell lines (red arrows). Sections are counterstained with DAPI. Scale bars: 100 µm. For *Oct4ΔObs;Otx2ER^{T2}* and *NanogΔObs3;Otx2ER^{T2}* mutants, two independent clones were analysed. (E) RT-qPCR analysis performed at d2 to determine the expression level of *Prdm14* and *Blimp1* in all cell lines. Data were normalized to *Tbp* mRNA and are reported as the mean±s.d. of three independent experiments.

Development (2021) 148, dev199166. doi:10.1242/dev.199166

sections and cytospin experiments, or transferred to ultralow adhesion 24-well plates (Corning) where they were incubated in the same culture media for an additional 4 days before FACS analysis. Medium was replaced every other day. Culture conditions for cell aggregates were based on the method reported by Hayashi et al. (2011).

In protocol 1, cell aggregates were cultured in GK15 supplemented with LIF (1000 U/ml), bone morphogenetic protein 4 (BMP4) (50 ng/ml), BMP8A (50 ng/ml), stem cell factor (SCF) (10 ng/ml) (all from R&D Systems) and epidermal growth factor (EGF) (10 ng/ml) (PeproTech) (Zhang et al., 2018; Hayashi et al., 2011) (Figs 1B and 2A). Protocol 2 differed from protocol 1 in that ESCs were maintained in FBS+LIF (Fig. 2I). In protocol 3, cell aggregates were cultured in only GK15 medium (Fig. 3A). In protocol 4, cell aggregates were cultured in GK15 with LIF (1000 U/ml) only (Fig. 4A). In protocol 5, cell aggregates were cultured in GK15 supplemented with BMP4 (50 ng/ml), BMP8A (50 ng/ml), SCF (10 ng/ml) and EGF (10 ng/ml), and without LIF (Fig. 4F). In protocol 6, cell aggregates were cultured in GK15 supplemented with CHIR (3 µM) only (Fig. 5A). In protocol 7, cell aggregates were cultured in GK15 supplemented with LIF (1000 U/ml) and CHIR (3 µM) (Fig. 5F). In protocol 8, cell aggregates were cultured in GK15 supplemented with LIF (1000 U/ml) and low doses of BMP4 (5 ng/ml), BMP8A (5 ng/ml), SCF (1 ng/ml) and EGF (1 ng/ml) (Fig. 6A). In protocol 9, cell aggregates were cultured in GK15 supplemented with LIF (1000 U/ml) and CHIR (3 µM), and low doses of BMP4 (5 ng/ml), BMP8A (5 ng/ml), SCF (1 ng/ml) and EGF (1 ng/ml) (Fig. 6F).

Two additional culture conditions without LIF were employed as control experiments: in the first condition, cell aggregates were cultured in GK15 supplemented with low doses of BMP4 (5 ng/ml), BMP8A (5 ng/ml), SCF (1 ng/ml) and EGF (1 ng/ml) (Fig. S6A); in the second condition, cell aggregates were cultured in GK15 supplemented with CHIR (3 µM) and low doses of BMP4 (5 ng/ml), BMP8A (5 ng/ml), SCF (1 ng/ml) and EGF (1 ng/ml) (Fig. S6D).

For experiments performed to assess the effect of different concentrations of LIF, wild-type and mutant cell aggregates were cultured according to the standard and modified versions of protocols 4 and 9. For protocol 4, cell aggregates were cultured for 6 days in GK15 medium supplemented with 300, 1000 (standard protocol 4) and 3000 U/ml of LIF only (Fig. S7A,B); for protocol 9, cell aggregates were cultured in the presence of fixed concentrations of CHIR (3 µM) and low doses of BMP4 (5 ng/ml), BMP8A (5 ng/ml), SCF (1 ng/ml) and EGF (1 ng/ml) in combination with 300, 1000 (standard protocol 9) and 3000 U/ml of LIF (Fig. S7C,D).

For experiments involving *E14;Otx2ER^{T2}*, *Oct4ΔObs;Otx2ER^{T2}*, *NanogΔObs3;Otx2ER^{T2}* and *Otx2KO;Otx2ER^{T2}* cell lines, Tx (200 nM) was administered from d0 to d2 of the cell aggregation phase both for FACS experiments on d6 and immunohistochemistry and RT-qPCR analyses on d2. For these cell lines, EpiLC-derived cell aggregates were cultured following protocol 1 conditions.

Alkaline phosphatase assay, and FGF2 and LIF response experiments

For alkaline phosphatase (ALP) staining, 8×10^2 ESCs cultured in FBS+LIF medium were seeded as triplicates in six-well plates and grown for 5 days. Upon fixation in 10% neutral buffered formalin (Sigma), ALP activity was revealed by 30 min incubation in a freshly made solution containing 0.1 M Tris-HCl (pH 8.3), Naphthol AS MX-PO_4 (5 mg, pre-dissolved in 200 µl of N,N-Dimethylformamide) as phosphatase substrate and Fast Red Violet (30 mg) as a dye (both from Sigma) in a 50 ml final volume. After a few

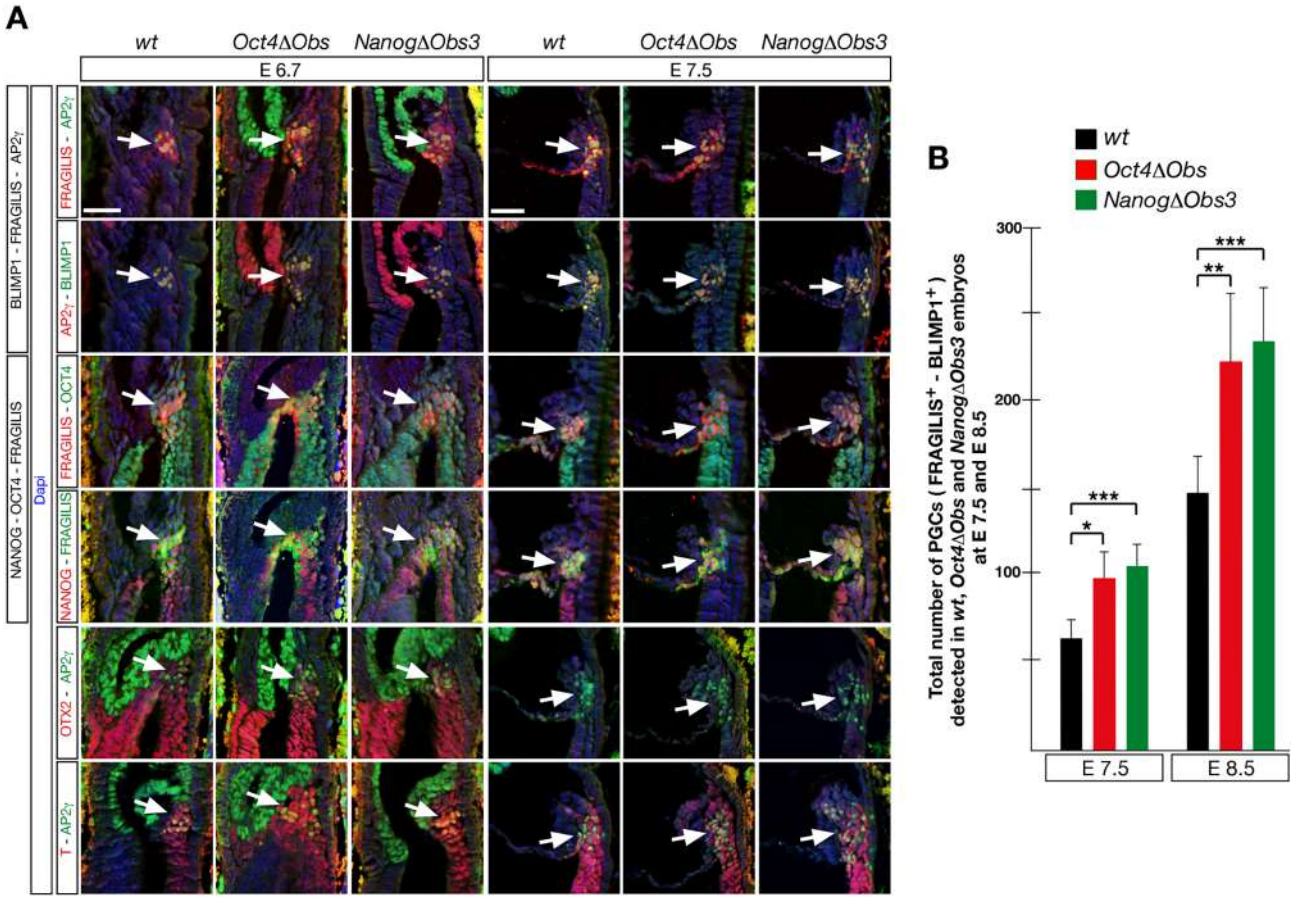

Fig. 8. Increased generation of PGCs in Δ*Obs* mutant embryos. (A) Immunohistochemistry analysis of wild-type and Δ*Obs* homozygous embryos at E6.7 and E7.5 using the indicated antibodies. Sections are counterstained with DAPI. Arrows indicate PGCs. Scale bars: 50 µm. (B) PGC counting data collected in wild-type and Δ*Obs* embryos at E7.5 and E8.5. The number of PGCs is reported as mean±s.d. **P*=0.001-0.005, ***P*<0.001 and ****P*<0.0005.

Development (2021) 148, dev199166. doi:10.1242/dev.199166

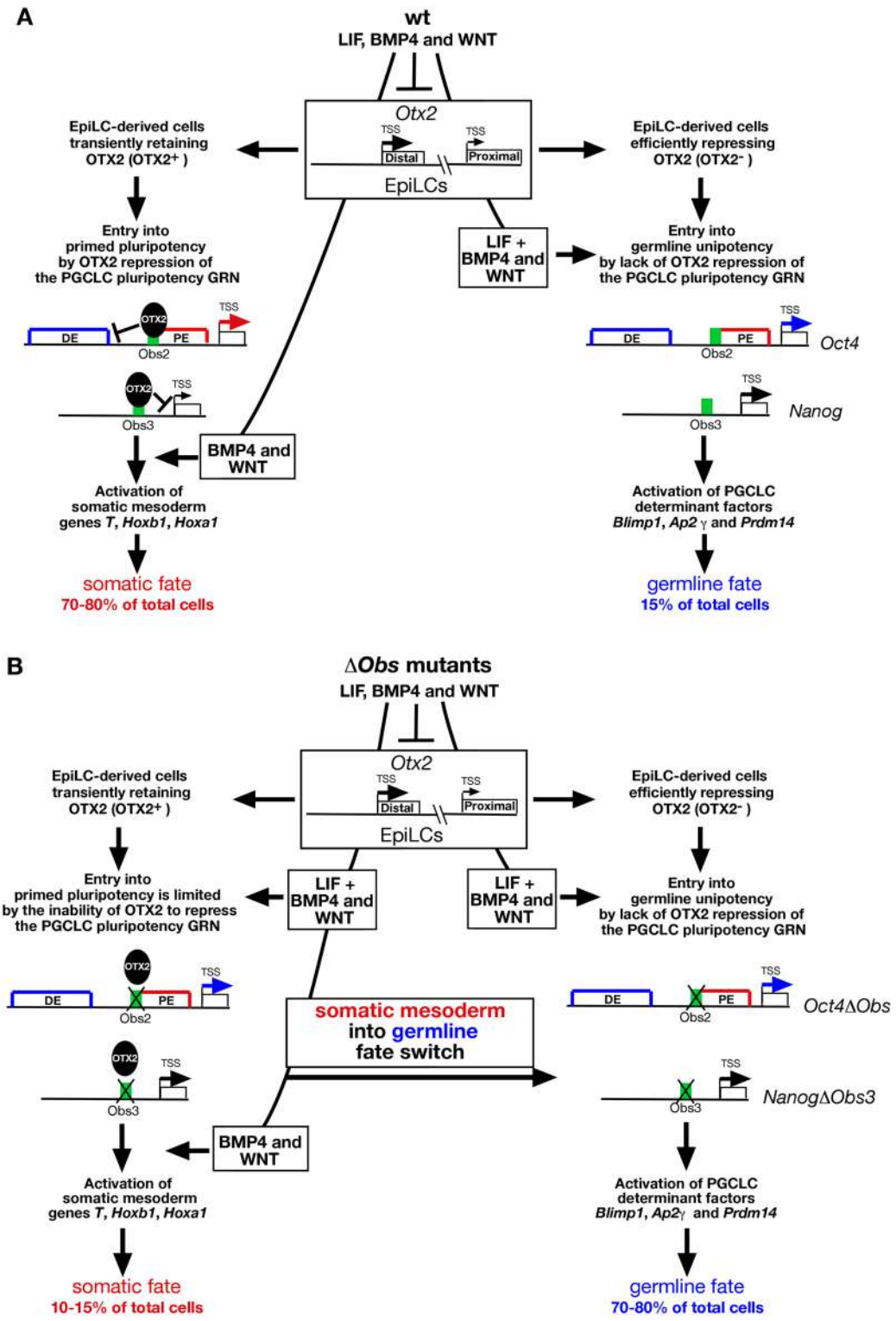

Fig. 9. Model of OTX2 action in germline and somatic mesoderm differentiation. Diagram illustrating the role of OTX2 in controlling the contribution of EpiLC-derived cells to germline and somatic mesoderm. (A) During the cell aggregation phase, *Otx2* suppression by LIF, BMP4 and WNT generates OTX2$^+$ and OTX2$^-$ cell subtypes. OTX2$^-$ cells (on the right) activate the PGCLC pluripotency GRN and, supported by cytokine-dependent stimulation of proliferation, enter the germline differentiation program to generate PGCLCs in 15% of the population; OTX2$^+$ cells (on the left) enter primed pluripotency via OTX2-mediated repression of the PGCLC pluripotency GRN and generate somatic mesoderm cells in about 70-80% of the population. (B) In Δ*Obs* mutants, the initial steps giving rise to the OTX2$^-$ and OTX2$^+$ cell subtypes, and the germline fate of the OTX2$^-$ cell subtype (on the right) are apparently unaffected. In contrast, entry into primed pluripotency of the OTX2$^+$ cell subtype (on the left) is limited by the inability of OTX2 to repress the pluripotency GRN, which, together with cytokines, promotes germline differentiation. This is reflected by a switch from somatic into germline fate in both Δ*Obs* mutants. The distal and proximal transcription start sites (TSSs) of *Otx2* are indicated. The DE and PE of *Oct4* are framed in blue and red, with the blue and red horizontal arrows corresponding to *Oct4* transcripts driven by the DE and PE, respectively. The size of the horizontal arrows indicating the TSS of *Nanog* and TSSs of *Otx2* are proportional to the transcriptional activity. The green boxes correspond to Obs2 for *Oct4* and to Obs3 for *Nanog*.

Development (2021) 148, dev199166. doi:10.1242/dev.199166

washes in water, colonies were scored as those exhibiting homogeneous staining and counted. For LIF response experiments, ESCs were kept for up to 1 h in GMEM containing 15% KSR in the absence of LIF, which was then added back to the medium at a concentration of 10^3 Units/ml. p-STAT3 was monitored after 20 min by western blots (Acampora et al., 2017). For the FGF2 response, ESCs were washed and kept in GMEM containing 5% KSR with or without FGF2 at a concentration of 5 ng/ml for 15 and 45 min (Acampora et al., 2016). The FGF2 response was determined by assessing the level of p-ERK1,2 in western blots.

ChIP experiments

ChIP experiments were performed as previously described (Lee et al., 2006) on wild-type and *Otx2KO* ESCs and EpiLCs with a rabbit polyclonal OTX2 antibody (Acampora et al., 2016), and on d2 cell aggregates with a rabbit histone H3 tri-methyl lysine 9 (H3K9me3) antibody and normal rabbit IgG. On the day before chromatin preparation, protein A dynabeads (Invitrogen) were washed three times with PBS containing 0.5% BSA and pre-adsorbed overnight with the different antibodies and normal rabbit IgG. For aggregates only, cells were washed with PBS and trypsinized before fixation. Formaldehyde (1%) crosslinked cells were then quenched with 125 mM glycine and washed twice with ice-cold PBS. Upon collection and centrifugation at 4°C, cells were lysed in LB1 buffer (50 mM Hepes-KOH, 140 mM NaCl, 1 mM EDTA, 10% glycerol, 0.5% NP-40 and 0.25% Triton X-100), then resuspended in LB2 buffer [10 mM Tris-HCl (pH 8.0), 200 mM NaCl, 1 mM EDTA and 0.5 mM EGTA] with rocking at 4°C for 10 min each time. Isolated nuclei were resuspended into LB3 buffer [10 mM Tris-HCl (pH 8), 100 mM NaCl, 1 mM EDTA, 0.5 mM EGTA, 0.1% Na-Deoxycholate and 0.5% N-lauroylsarcosine Na-salt] and kept on ice. All lysis buffers were prepared with freshly added protease inhibitor cocktail plus PMSF. Sonication was performed with a Misonix 2000 sonicator to obtain fragment size with a peak of ∼500 bp or 300 bp, respectively, for OTX2 or H3K9me3 ChIP assays. SDS 0.1% (only for OTX2 ChIP assays) and Triton X-100 (1%) were added to sonicated chromatin before centrifugation to remove debris. Supernatant was then incubated with the antibody- or IgG-coated beads on a rotator at 4°C for at least 18 h (Acampora et al., 2016). Beads were collected at any step through the magnetic stand and sequentially washed with low-salt solution [0.1% SDS, 1% Triton, 2 mM EDTA (pH 8), 20 mM Tris-HCl (pH 8) and 150 mM NaCl], high-salt solution [0.1% SDS, 1% Triton, 2 mM EDTA, 20 mM Tris-HCl (pH 8) and 500 mM NaCl], LiCl solution [0.25 M LiCl, 1% NP40, 1% Na-Deoxycholate and 10 mM Tris-HCl (pH 8)] and TE buffer [Tris-HCl 10 mM (pH 8) and 1 mM EDTA] containing 50 mM NaCl. Beads were then incubated for 15 min at 65°C with elution buffer [50 mM Tris-HCl (pH 8), 10 mM EDTA and 1% SDS]. The immunoprecipitated (IP) DNA was separated from the beads and reverse crosslinked along with input (non-IP DNA) by overnight incubation at 65°C. After RNA and protein digestion, DNA samples were purified by phenol-chloroform extraction and ethanol precipitation. DNA was resuspended in 10 mM Tris-HCl (pH 8) and used in standard qPCR reactions. Fold enrichment of OTX2 ChIP samples was calculated relative to ChIP in *Otx2KO* cells, used as a negative control, according to the $2^{-\Delta\Delta Ct}$ formula. ChIP values for H3K9me3 and control IgG were calculated as percentage of input, according to the formula: % Input=$2^{-\Delta Ct(\text{normalized ChIP})}$. Data are mean±s.d. of three independent experiments, each in technical triplicates. ChIP primers are listed in Table S5.

Immunocytochemistry and immunohistochemistry

For immunocytochemistry experiments on ESCs and EpiLCs, adherent cells grown on four-well chamber slides (Sarstedt) were PBS washed and fixed with 4% paraformaldehyde (PFA). Blocking (1 h) and incubation with primary antibodies (overnight) were performed in PBS containing 0.3% Triton X-100 and 2% skimmed milk powder (BioRad). Cells were washed three times with PBS before and after incubation with Alexa Fluor secondary antibodies (90 min). Cells were then counterstained with DAPI (Acampora et al., 2016). Immunohistochemistry experiments on d2 PGCLCs were performed on an average of 100-150 cell aggregates per experiment. After washing in PBS, cell aggregates were fixed overnight in 4% PFA, then dehydrated and processed for paraffin wax embedding and microtome sectioning. Slides were then xylene deparaffinized and rehydrated through a descending series of alcohol to water before being boiled in citrate buffer (pH 6.0) for antigen retrieval. Sections were then incubated with a blocking solution containing 0.5% milk, 10% FBS and 1% BSA, and hybridized with the primary and Alexa Fluor secondary antibodies as described before (Acampora et al., 2013). For immunostaining of cytospin preparations, d2 cell aggregates were collected, washed twice with PBS, dissociated with trypsin and resuspended in 5% FBS in PBS to obtain a single cell suspension. After centrifugation, cells were resuspended at 1×10^6 cells/ml in 1% BSA in PBS and 2×10^5 cells were loaded onto cytofunnels and centrifuged for 7 min at 1200 ***g*** Cells were fixed in 4% PFA and processed for immunostaining as described for ESCs and EpiLCs.

For *in vivo* PGC counting, embryos obtained from natural matings of age-matched (3 months old) randomly selected breeding pairs of wild-type and Δ*Obs* mutants were collected at E7.5 and E8.5, fixed overnight in 4% PFA in PBS, dehydrated, paraffin wax embedded and sectioned. Embryos matched for morphology or number of somites, were processed for immunostaining with fragilis and BLIMP1 antibodies as for cell aggregates. All sections, including PGCs, were selected and captured for cell counting. All immunostaining images were captured with a Nikon eclipse NI microscope. For immunohistochemistry experiments performed with three compatible antibodies, fluorescence was excited at 405 nm for DAPI and at 488 nm, 555 nm and 647 nm for secondary antibodies. Eventually, red colour for fluorescence excited at 555 nm was converted to green pseudocolour to allow merging of all combinations. All antibodies employed for immunostaining experiments are listed in Table S6.

Cell counting and statistical analysis

Cytospin assays were immunostained and three non-overlapping fields per experiment were captured, images were printed in A4 format and cell number manually determined. Standard deviation (s.d.) was calculated from the analysis of three independent experiments for each differentiation protocol and for each cell line (Tables S2 and S3). Similarly, also for PGC counting in embryos, immunostained sections were selected, captured, printed in A4 format and fragilis$^+$-BLIMP1$^+$ cells counted. Embryos were selected by morphology at E7.5, and by morphology and number of somites at E8.5. Standard deviation was determined by the analysis of six and seven embryos/genotype, respectively, at E7.5 and E8.5 (Table S4). *P* values were determined by using the one-tailed or two-tailed unpaired Student's *t*-test.

Flow cytometry

FACS analysis was performed on d6 cell aggregates. An average of 50-60 aggregates were collected and dissociated into single cells with trypsin and neutralized in PBS containing 10% FBS. A maximum of 5×10^5 cells were collected by centrifugation and the pellet resuspended in 100 µl PBS plus 10% FBS supplemented with Alexa Fluor 647 anti-mouse/human CD15 (SSEA1) (Biolegend) and PE anti-mouse/rat CD61 (Biolegend) (Zhang et al., 2018), diluted 1/200 and 1/500, respectively, and incubated for 30 min at 4°C. Cells were washed twice in 1 ml PBS plus 10% FBS before analysis on a BD FACSAria III (Becton Dickinson). Data were acquired using BD FACSDiva software 8.0.1 and analysed using FlowJo software version 10.7.1. Gating strategy is shown in Fig. S3A. The dissociated cell population was first gated on the basis of the FSC (size) and SSC (complexities) scatter plot; singlets were then selected based on the linear correlation between the FSC area (FSC-A) and the FSC height (FSC-H); dead cells were excluded by 7-AAD dye (Fig. S3A-C). All FACS assays were performed in at least three independent experiments.

Chimaerism assay

c57BL/6 blastocysts were injected with *Oct4*Δ*Obs* ESCs (n=10 cells/embryo) for a total of 50 embryos and transferred into B6D2F1 foster mothers. Chimaerism was assessed by extent of coat colour mosaicism.

RNA extraction, cDNA synthesis and RT-qPCR experiments

Total RNA was extracted from cell lysates using TRIzol Reagent (Invitrogen) and reverse transcribed using Superscript II (Invitrogen)

according to the manufacturer's instructions. First-strand cDNA was used for RT-qPCR analysis using Power SYBR Green Master Mix (Applied Biosystems). RT-qPCR experiments were performed on RNA extracted from about 80 cell aggregates per time point (from EpiLC, until day 2) for protocols 1 and 3-9, using primers specific for *Otx2*, *Oct4*, *Nanog*, *Ap2γ*, *Blimp1*, *T* and *Hoxb1*. RT-qPCR experiments were also performed on RNA extracted from SSEA1^{+}-CD61^{+} cells, FACS-sorted with the same gating strategy previously described at day 6 for PGCLC differentiation in protocols 1 and 9. For SSEA1^{+}-CD61^{+} sorted cells, primers were specific for *Blimp1*, *Prdm14*, *Ap2γ*, *Nanos3*, *Ddx4* (also known as *Mvh*), *Prmt5*, fragilis, *Alpl* (also known as *Tnap*), *Gcna1*, *Dazl* (also known as *Dazla*) and *Kit*. Gene expression was normalized to TATA-box binding protein (*Tbp*) transcripts according to the $2^{(Ct\ TBP - Ct\ target)}$ formula. Experiments were performed as biological triplicates and technical duplicates. Oligonucleotide sequences for RT-qPCR analysis are listed in Table S5.

Western blot assay

Total cell lysates were loaded and run on a 10.5% SDS-PAGE gel. Proteins were transferred onto Protran nitrocellulose membranes (GE Healthcare), blocked in 5% skimmed milk (BioRad) for 1 h at room temperature and incubated with primary antibodies (4°C, overnight). PBS plus Tween 20 washes were carried out before and after secondary antibody incubation (1 h at room temperature). Protein expression was revealed by ECL reactions (GE Healthcare). Western Blot antibodies are listed in Table S6.

Acknowledgements

We thank members of the I.C. lab and V. Wilson for comments on the manuscript, L. Pisapia for support with FACS data analysis, and the staff of the IGB animal house and IGB FACS facility. We also thank D. Graniero for typing and formatting the manuscript.

Competing interests

The authors declare no competing or financial interests.

Author contributions

Conceptualization: L.G.D.G., D.A.; Methodology: L.G.D.G., D.A., D.O.; Formal analysis: V.N.; Investigation: L.G.D.G., D.A., D.O., P.B., E.B.; Writing - original draft: D.A., A.S.; Writing - review & editing: I.C., A.S.; Supervision: A.S.; Funding acquisition: A.S.

Funding

This work was supported by the Fondo Europeo di Sviluppo Regionale (SATIN-POR CAMPANIA FESR 2014/2020) and the PRIN project from the Ministero dell'Istruzione, dell'Universita' e della Ricerca (20157JF8P5_004 to A.S.), and by the Medical Research Council (MR/T003162/1 to I.C.). E.B. is supported by a Marie Skłodowska-Curie fellowship (H2020-MSCA-IF-2018/843879).

Peer review history

The peer review history is available online at https://journals.biologists.com/dev/article-lookup/doi/10.1242/dev.199166

References

Acampora, D., Mazan, S., Lallemand, Y., Avantaggiato, V., Maury, M., Simeone, A. and Brûlet, P. (1995). Forebrain and midbrain regions are deleted in Otx2$^{-/-}$ mutants due to a defective anterior neuroectoderm specification during gastrulation. *Development* **121**, 3279-3290.

Acampora, D., Di Giovannantonio, L. G. and Simeone, A. (2013). Otx2 is an intrinsic determinant of the embryonic stem cell state and is required for transition to a stable epiblast stem cell condition. *Development* **140**, 43-55. doi:10.1242/dev.085290

Acampora, D., Omodei, D., Petrosino, G., Garofalo, A., Savarese, M., Nigro, V., Di Giovannantonio, L. G., Mercadante, V. and Simeone, A. (2016). Loss of the Otx2-binding site in the Nanog promoter affects the integrity of embryonic stem cell subtypes and specification of inner cell mass-derived epiblast. *Cell Rep.* **15**, 2651-2664. doi:10.1016/j.celrep.2016.05.041

Acampora, D., Di Giovannantonio, L. G., Garofalo, A., Nigro, V., Omodei, D., Lombardi, A., Zhang, J., Chambers, I. and Simeone, A. (2017). Functional antagonism between OTX2 and NANOG specifies a spectrum of heterogeneous identities in embryonic stem cells. *Stem Cell Rep.* **9**, 1642-1659. doi:10.1016/j.stemcr.2017.09.019

Ancelin, K., Lange, U. C., Hajkova, P., Schneider, R., Bannister, A. J., Kouzarides, T. and Surani, M. A. (2006). Blimp1 associates with Prmt5 and directs histone arginine methylation in mouse germ cells. *Nat. Cell Biol.* **8**, 623-630. doi:10.1038/ncb1413

Aramaki, S., Hayashi, K., Kurimoto, K., Ohta, H., Yabuta, Y., Iwanari, H., Mochizuki, Y., Hamakubo, T., Kato, Y., Shirahige, K. et al. (2013). A mesodermal factor, T, specifies mouse germ cell fate by directly activating germline determinants. *Dev. Cell* **27**, 516-529. doi:10.1016/j.devcel.2013.11.001

Buecker, C., Srinivasan, R., Wu, Z., Calo, E., Acampora, D., Faial, T., Simeone, A., Tan, M., Swigut, T. and Wysocka, J. (2014). Reorganization of enhancer patterns in transition from naive to primed pluripotency. *Cell Stem Cell* **14**, 838-853. doi:10.1016/j.stem.2014.04.003

Campolo, F., Gori, M., Favaro, R., Nicolis, S., Pellegrini, M., Botti, F., Rossi, P., Jannini, E. A. and Dolci, S. (2013). Essential role of Sox2 for the establishment and maintenance of the germ cell line. *Stem Cells* **31**, 1408-1421. doi:10.1002/stem.1392

Chambers, I., Silva, J., Colby, D., Nichols, J., Nijmeijer, B., Robertson, M., Vrana, J., Jones, K., Grotewold, L. and Smith, A. (2007). Nanog safeguards pluripotency and mediates germline development. *Nature* **450**, 1230-1234. doi:10.1038/nature06403

Cheng, L., Gearing, D. P., White, L. S., Compton, D. L., Schooley, K. and Donovan, P. J. (1994). Role of leukemia inhibitory factor and its receptor in mouse primordial germ cell growth. *Development* **120**, 3145-3153.

Choi, H. W., Joo, J. Y., Hong, Y. J., Kim, J. S., Song, H., Lee, J. W., Wu, G., Schöler, H. R. and Do, J. T. (2016). Distinct enhancer activity of Oct4 in naive and primed mouse pluripotency. *Stem Cell Rep.* **7**, 911-926. doi:10.1016/j.stemcr.2016.09.012

Farini, D., Scaldaferri, M. L., Iona, S., La Sala, G. and De Felici, M. (2005). Growth factors sustain primordial germ cell survival, proliferation and entering into meiosis in the absence of somatic cells. *Dev. Biol.* **285**, 49-56. doi:10.1016/j.ydbio.2005.06.036

Günesdogan, U. and Surani, M. A. (2016). Developmental competence for primordial germ cell fate. *Curr. Top. Dev. Biol.* **117**, 471-496. doi:10.1016/bs.ctdb.2015.11.007

Hackett, J. A. and Surani, M. A. (2014). Regulatory principles of pluripotency: from the ground state up. *Cell Stem Cell* **15**, 416-430. doi:10.1016/j.stem.2014.09.015

Hayashi, K., de Sousa Lopes, S. M. C. and Surani, M. A. (2007). Germ cell specification in mice. *Science* **316**, 394-396. doi:10.1126/science.1137545

Hayashi, K., Ohta, H., Kurimoto, K., Aramaki, S. and Saitou, M. (2011). Reconstitution of the mouse germ cell specification pathway in culture by pluripotent stem cells. *Cell* **146**, 519-532. doi:10.1016/j.cell.2011.06.052

Hayashi, K., Ogushi, S., Kurimoto, K., Shimamoto, S., Ohta, H. and Saitou, M. (2012). Offspring from oocytes derived from in vitro primordial germ cell-like cells in mice. *Science* **338**, 971-975. doi:10.1126/science.1226889

Hayashi, M., Kawaguchi, T., Durcova-Hills, G. and Imai, H. (2017). Generation of germ cells from pluripotent stem cells in mammals. *Reprod. Med. Biol.* **17**, 107-114. doi:10.1002/rmb2.12077

Johnson, A. D. and Alberio, R. (2015). Primordial germ cells: the first cell lineage or the last cells standing? *Development* **142**, 2730-2739. doi:10.1242/dev.113993

Johnson, A. D., Crother, B., White, M. E., Patient, R., Bachvarova, R. F., Drum, M. and Masi, T. (2003). Regulative germ cell specification in axolotl embryos: a primitive trait conserved in the mammalian lineage. *Philos. Trans. R. Soc. Lond. B Biol. Sci.* **358**, 1371-1379. doi:10.1098/rstb.2003.1331

Karwacki-Neisius, V., Göke, J., Osorno, R., Halbritter, F., Ng, J. H., Weiße, A. Y., Wong, F. C. K., Gagliardi, A., Mullin, N. P., Festuccia, N. et al. (2013). Reduced Oct4 expression directs a robust pluripotent state with distinct signaling activity and increased enhancer occupancy by Oct4 and Nanog. *Cell Stem Cell* **12**, 531-545. doi:10.1016/j.stem.2013.04.023

Kehler, J., Tolkunova, E., Koschorz, B., Pesce, M., Gentile, L., Boiani, M., Lomelí, H., Nagy, A., McLaughlin, K. J., Schöler, H. R. et al. (2004). Oct4 is required for primordial germ cell survival. *EMBO Rep.* **5**, 1078-1083. doi:10.1038/sj.embor.7400279

Koshimizu, U., Taga, T., Watanabe, M., Saito, M., Shirayoshi, Y., Kishimoto, T. and Nakatsuji, N. (1996). Functional requirement of gp130-mediated signaling for growth and survival of mouse primordial germ cells in vitro and derivation of embryonic germ (EG) cells. *Development* **122**, 1235-1242.

Kurimoto, K., Yabuta, Y., Ohinata, Y., Shigeta, M., Yamanaka, K. and Saitou, M. (2008). Complex genome-wide transcription dynamics orchestrated by Blimp1 for the specification of the germ cell lineage in mice. *Genes Dev.* **22**, 1617-1635. doi:10.1101/gad.1649908

Laird, D. J. (2018). How to lose your inheritance. *Nature* **562**, 497-498. doi:10.1038/d41586-018-06849-5

Lawson, K. A., Dunn, N. R., Roelen, B. A. J., Zeinstra, L. M., Davis, A. M., Wright, C. V. E., Korving, J. P. W. F. M. and Hogan, B. L. (1999). Bmp4 is required for the generation of primordial germ cells in the mouse embryo. *Genes Dev.* **13**, 424-436. doi:10.1101/gad.13.4.424

Lee, T. I., Johnstone, S. E. and Young, R. A. (2006). Chromatin immunoprecipitation and microarray-based analysis of protein location. *Nat. Protoc.* **1**, 729-748. doi:10.1038/nprot.2006.98

Leitch, H. G., Nichols, J., Humphreys, P., Mulas, C., Martello, G., Lee, C., Jones, K., Surani, M. A. and Smith, A. (2013). Rebuilding pluripotency from primordial germ cells. *Stem Cell Rep.* **1**, 66-78. doi:10.1016/j.stemcr.2013.03.004

Magnúsdóttir, E., Dietmann, S., Murakami, K., Günesdogan, U., Tang, F., Bao, S., Diamanti, E., Lao, K., Gottgens, B. and Azim Surani, M. (2013). A tripartite transcription factor network regulates primordial germ cell specification in mice. *Nat. Cell Biol.* **15**, 905-915. doi:10.1038/ncb2798

Matsuda, T., Nakamura, T., Nakao, K., Arai, T., Katsuki, M., Heike, T. and Yokota, T. (1999). STAT3 Activation is sufficient to maintain an undifferentiated state of mouse embryonic stem cells. *EMBO J.* **18**, 4261-4269. doi:10.1093/emboj/18.15.4261

Murakami, K., Günesdogan, U., Zylicz, J. J., Tang, W. W. C., Sengupta, R., Kobayashi, T., Kim, S., Butler, R., Dietmann, S. and Surani, M. A. (2016). NANOG alone induces germ cells in primed epiblast in vitro by activation of enhancers. *Nature* **529**, 403-407. doi:10.1038/nature16480

Nakaki, F., Hayashi, K., Ohta, H., Kurimoto, K., Yabuta, Y. and Saitou, M. (2013). Induction of mouse germ-cell fate by transcription factors in vitro. *Nature* **501**, 222-226. doi:10.1038/nature12417

Neagu, A., van Genderen, E., Escudero, I., Verwegen, L., Kurek, D., Lehmann, J., Stel, J., Dirks, R. A. M., van Mierlo, G., Maas, A. et al. (2020). In vitro capture and characterization of embryonic rosette-stage pluripotency between naive and primed states. *Nat. Cell Biol.* **22**, 534-545. doi:10.1038/s41556-020-0508-x

Niwa, H., Ogawa, K., Shimosato, D. and Adachi, K. (2009). A parallel circuit of LIF signaling pathways maintains pluripotency of mouse ES cells. *Nature* **460**, 118-122. doi:10.1038/nature08113

Ogawa, K., Nishinakamura, R., Iwamatsu, Y., Shimosato, D. and Niwa, H. (2006). Synergistic action of Wnt and LIF in maintaining pluripotency of mouse ES cells. *Biochem. Biophys. Res. Commun.* **343**, 159-166. doi:10.1016/j.bbrc.2006.02.127

Ohinata, Y., Payer, B., O'Carroll, D., Ancelin, K., Ono, Y., Sano, M., Barton, S. C., Obukhanych, T., Nussenzweig, M., Tarakhovsky, A. et al. (2005). Blimp1 is a critical determinant of the germ cell lineage in mice. *Nature* **436**, 207-213. doi:10.1038/nature03813

Ohinata, Y., Ohta, H., Shigeta, M., Yamanaka, K., Wakayama, T. and Saitou, M. (2009). A signaling principle for the specification of the germ cell lineage in mice. *Cell* **137**, 571-584. doi:10.1016/j.cell.2009.03.014

Okamura, D., Tokitake, Y., Niwa, H. and Matsui, Y. (2008). Requirement of Oct3/4 function for germ cell specification. *Dev. Biol.* **317**, 576-584. doi:10.1016/j.ydbio.2008.03.002

Saitou, M. (2009). Germ cell specification in mice. *Curr. Opin. Genet. Dev.* **19**, 386-395. doi:10.1016/j.gde.2009.06.003

Saitou, M. and Yamaji, M. (2012). Primordial germ cells in mice. *Cold Spring Harb. Perspect. Biol.* **4**, a008375. doi:10.1101/cshperspect.a008375

Saitou, M., Barton, S. C. and Surani, M. A. (2002). A molecular programme for the specification of germ cell fate in mice. *Nature* **418**, 293-300. doi:10.1038/nature00927

Saitou, M., Payer, B., O'Carroll, D., Ohinata, Y. and Surani, M. A. (2005). Blimp1 and the emergence of the germ line during development in the mouse. *Cell Cycle* **4**, 1736-1740. doi:10.4161/cc.4.12.2209

Senft, A. D., Bikoff, E. K., Robertson, E. J. and Costello, I. (2019). Genetic dissection of Nodal and Bmp signaling requirements during primordial germ cell development in mouse. *Nat. Commun.* **10**, 1-11. doi:10.1038/s41467-019-09052-w

Smith, A. (2017). Formative pluripotency: the executive phase in a developmental continuum. *Development* **144**, 365-373. doi:10.1242/dev.142679

Surani, M. A. (2001). Reprogramming of genome function through epigenetic inheritance. *Nature* **414**, 122-128. doi:10.1038/35102186

Surani, M. A., Hayashi, K. and Hajkova, P. (2007). Genetic and epigenetic regulators of pluripotency. *Cell* **128**, 747-762. doi:10.1016/j.cell.2007.02.010

ten Berge, D., Kurek, D., Blauwkamp, T., Koole, W., Maas, A., Eroglu, E., Siu, R. K. and Nusse, R. (2011). Embryonic stem cells require Wnt proteins to prevent differentiation to epiblast stem cells. *Nat. Cell. Biol.* **13**, 1070-1075. doi:10.1038/ncb2314

Vincent, S. D., Dunn, N. R., Sciammas, R., Shapiro-Shalef, M., Davis, M. M., Calame, K., Bikoff, E. K. and Robertson, E. J. (2005). The zinc finger transcriptional repressor Blimp1/Prdm1 is dispensable for early axis formation but is required for specification of primordial germ cells in the mouse. *Development* **132**, 1315-1325. doi:10.1242/dev.01711

Weber, S., Eckert, D., Nettersheim, D., Gillis, A. J. M., Schäfer, S., Kuckenberg, P., Ehlermann, J., Werling, U., Biermann, K., Looijenga, H. J. et al. (2010). Critical function of AP-2 gamma/TCFAP2C in mouse embryonic germ cell maintenance. *Biol. Reprod.* **82**, 214-223. doi:10.1095/biolreprod.109.078717

Wu, G. and Schöler, H. R. (2014). Role of Oct4 in the early embryo development. *Cell. Regen.* **3**, 3-7.

Wylie, C. (1999). Germ cells. *Cell* **96**, 165-174. doi:10.1016/S0092-8674(00)80557-7

Yamaguchi, S., Kurimoto, K., Yabuta, Y., Sasaki, H., Nakatsuji, N., Saitou, M. and Tada, T. (2009). Conditional knockdown of Nanog induces apoptotic cell death in mouse migrating primordial germ cells. *Development* **136**, 4011-4020. doi:10.1242/dev.041160

Yamaji, M., Seki, Y., Kurimoto, K., Yabuta, Y., Yuasa, M., Shigeta, M., Yamanaka, K., Ohinata, Y. and Saitou, M. (2008). Critical function of Prdm14 for the establishment of the germ cell lineage in mice. *Nat. Genet.* **40**, 1016-1022. doi:10.1038/ng.186

Yang, S.-H., Kalkan, T., Morissroe, C., Marks, H., Stunnenberg, H., Smith, A. and Sharrocks, A. D. (2014). Otx2 and Oct4 drive early enhancer activation during embryonic stem cell transition from naive pluripotency. *Cell Rep.* **7**, 1968-1981. doi:10.1016/j.celrep.2014.05.037

Yeom, Y. I., Fuhrmann, G., Ovitt, C. E., Brehm, A., Ohbo, K., Gross, M., Hübner, K. and Schöler, H. R. (1996). Germline regulatory element of Oct-4 specific for the totipotent cycle of embryonal cells. *Development* **122**, 881-894.

Ying, Q.-L., Nichols, J., Chambers, I. and Smith, A. (2003). BMP induction of Id proteins suppresses differentiation and sustains embryonic stem cell self-renewal in collaboration with STAT3. *Cell* **115**, 281-292. doi:10.1016/S0092-8674(03)00847-X

Ying, Q.-L., Wray, J., Nichols, J., Batlle-Morera, L., Doble, B., Woodgett, J., Cohen, P. and Smith, A. (2008). The ground state of embryonic stem cell self-renewal. *Nature* **453**, 519-523. doi:10.1038/nature06968

Zhang, M. and Chambers, I. (2019). Segregation of the mouse germline and soma. *Cell Cycle* **18**, 3064-3071. doi:10.1080/15384101.2019.1672466

Zhang, J., Zhang, M., Acampora, D., Vojtek, M., Yuan, D., Simeone, A. and Chambers, I. (2018). OTX2 restricts entry to the mouse germline. *Nature* **562**, 595-599. doi:10.1038/s41586-018-0581-5